SEQUENCE STRATIGRAPHY OF THE MIDDLE CRETACEOUS WOODBINE AND EAGLE FORD GROUPS IN THE NORTHWEST EAST TEXAS BASIN

A Thesis

by

LEAH NICOLE EVANS

Submitted to the Office of Graduate and Professional Studies of
Texas A&M University
in partial fulfillment of the requirements for the degree of

MASTER OF SCIENCE

Chair of Committee,	Michael Pope
Co-Chair of Committee,	Arthur Donovan
Committee Member,	Anthony Filippi
Head of Department,	Julie Newman

December 2022

Major Subject: Geology

ABSTRACT

Petrophysical, geochemical, and isotopic characteristics were used to define unconformity-bounded formations and members within the Woodbine and Eagle Ford Groups in the shallow subsurface along the northwestern margin of the East Texas Basin (ETB). These unconformity-bounded strata were mapped in the deeper subsurface portions of the ETB to define plays within these groups throughout the basin.

The K600sb marks the base of the Woodbine Group. This unconformity displays angular discordance that truncates the Buda Formation to the north and the west, controlling the limits of Buda Formation play fairways. The K615ts subdivides the Woodbine Group into the more sandstone-prone Dexter Formation (below) from the more mudstone-prone Lewisville Formation (above).

In the Dallas area, the K630sb marks the base of the Eagle Ford Group and occurs at the base of the "Tarrant Beds". This surface shows angular discordance and is geochemically distinct, based on X-Ray Fluorescence (XRF) data. The change to fossiliferous marine strata above is significant because the ammonite fauna of the Eagle Ford Group also occurs in the Cretaceous Western Interior Seaway, marking the time that the seaway first established. The K650sb subdivides the Eagle Ford Group into the more organic-, uranium, and carbonate-rich Lower Eagle Ford Formation (LEF) and organic- and uranium-poor, and argillaceous-rich Upper Eagle Ford Formation (UEF). This boundary controls the northern and eastern limits of the LEF unconventional reservoir play by truncation and geochemical data reveals a transition from anoxic sea-floor conditions (below) to oxic sea-floor conditions (above).

The interval between the K650sb and K670sb is the Lower Member of UEF (LM:UEF). Geochemical work indicates that the positive (δ13C) carbonate isotope excursion associated with the Cenomanian/Turonian Boundary Event (CTBE), which is also commonly termed the Ocean Anoxic Event 2 (OAE2), also coincides with this member. Regional correlations indicate that the major siliciclastic depocenter (delta system) within the LM:LEF is coeval to the classic Harris Delta System from the southern portions of the ETB. Paleogeographic maps of the LM:UEF in this study suggest that the sandstone-play fairway associated with the Harris Delta System is more regionally extensive than previously reported.

ACKNOWLEDGEMENTS

I thank Art Donovan, Michael Pope, Anthony Filippi, and many other people who have helped and supported me during my almost 6 years here at Texas A&M. I've learned what it means to be a geologist and ask the right questions that has allowed this study to be possible. I thank the USGS Gulf Coast Assessment Group for access to their cores, logs, and data and the Bureau of Economic Geology for use of their lab and well cuttings. Specifically, I am grateful to Scott Gifford, Molly McCreary, Chris Griffith, and Maria Gutierrez for their guidance. I thank Jenelle Wempner, Sidney Dangtran, Emily Dye, Deanna Flores, Kat Moore, Georgia McAdams, and Andress Ehrlich for their help and being such great friends. My project would have not been finished without the help of Andreas Kronenberg, Xiaofeng Chen, and Parker Johnson who helped fix the hydraulic press. Parker's encouragement and help is also a huge reason I have a completed thesis. I thank God that you were all put in my life when I needed you most.

Finally, I thank my family for supporting me as a geologist by stopping on the sides of roads to look at rocks and sending me pictures of outcrops on all their vacations. I will never get tired of answering your geology-related questions, even if I have answered them seventy times seven times. I hope you can be as proud of this work as I am.

CONTRIBUTORS AND FUNDING SOURCES

Contributors

My thesis committee consisted of Michael Pope [advisor] and Arthur Donovan [co-advisor] of the Department of Geology and Geophysics, and Anthony Filippi [committee member] of the Department of Geography. XRF data beyond that collected by me was collected by Molly McCreary.

Funding

I am thankful for the support from the Texas A&M University Unconventional Reservoirs Outcrop Characterization (UROC) Consortium and the Houston Geological Society (HGS) that made it possible for me to complete my work. I also thank Mr. and Mrs. Willard R. Green for sponsoring the Marianne W. & Willard R. Green Scholarship from the College of Geosciences and Marathon Oil Corporation for the Marathon Scholarship from the College of Geosciences.

TABLE OF CONTENTS

Page

LIST OF FIGURES

LIST OF TABLES

1. INTRODUCTION

During the onset of the Late Cretaceous (Cenomanian-Turonian), present-day Texas, the location for this study (Figure 1), was located at the southern gateway of the Cretaceous Western Interior Seaway (KWIS) positioned at the transition from a foreland basin to the west, and a tiered passive continental margin to the east. It was a time of peak global greenhouse conditions marked by expanded epicontinental seaways. Repeated episodes of ocean anoxia are reflected by the deposition of organic-rich source rocks. During this time, the Woodbine and Eagle Ford Groups, as well as the lowermost portions of the Austin Groups were sequentially deposited across Texas.

As illustrated on Figure 2A, during the Early Cenomanian, seas began to transgress the North American craton from the Gulf of Mexico to the south, and the Artic Ocean from the north. By the Earliest Turonian (Figure 2B), the period of peak global greenhouse conditions occurred, where eustatic sea-level was elevated approximately 500' (150 m) above current conditions (Donovan, personal communication), and the KWIS covered the craton from the Gulf of Mexico to the South to the Artic Ocean to the North. At this time, atmospheric CO2 was at least four times above present levels (Kaufman, 1995) ; and warm, more-equable climates, reflecting low thermal gradients, existed from the pole to the equator, as well as from top to bottoms in the world's ocean columns (Figure 2B).

Associated with the overall sea-level rise during the Cenomanian was the Cenomanian/Turonian Boundary Event (CTBE), also referred to as the Ocean Anoxic Event 2 (OAE2). The CTBE is an approximate 850,000-year-long period in the earth's history marked by the punctuated extinction of over half the world's Cretaceous ammonoid and brachiopod genera (Ogg and Hinnov, 2012). Geochemically, the CTBE is characterized by a globally recognized positive carbon isotope ($\delta^{13}C$) excursion (Figure 3) reflecting widespread removal of C12-enriched

organic matter in marine sediments and denoting one of the major global perturbations in the carbon cycle of the earth's paleo-oceans (Ma *et al.*, 2014). For geoscientist today, the CTBE, with its distinctive $\delta^{13}C$ signature, provides a useful chronostratigraphic maker suitable for regional and inter-regional correlations within Middle Cretaceous successions around the globe.

Within the Upper Cretaceous succession across the United States, the most prolific hydrocarbon bearing-system occurs within the East Texas Basin (ETB), where the supergiant East Texas Field is located (Halbouty, 1991). In the East Texas Field, fluvial-deltaic reservoirs of the Woodbine Group serve as conventional reservoirs, Eagle Ford strata as the source rocks, and the overlying Austin Group is the seal and trap (Halbouty, 1991). Toward the end of the 20th century, however, production in the ETB began to switch toward unconventional reservoirs. This started with the Austin Chalk in the mid 1980's as Sun Exploration and Production Company, successfully utilized modern horizontal drilling techniques to exploit the fractured Austin Chalk Play (Zuckerman, 2014). More recently, industry has utilized horizontal wells and fracking to unlock tight rock plays within strata (Hentz, Ambrose and Smith, 2014), defined herein, within the Eagle Ford Group. In fact, the future resource potential of the Eagle Ford Group was estimated undiscovered, technically recoverable, mean resources of the Eagle Ford Group, and associated Cenomanian-Turonian strata, in Gulf Coast Region of Texas, at 8.5 billion barrels of oil, 66 trillion cubic feet of natural gas, and 1.9 billion barrels of Natural Gas Liquids (NGL's) (Whidden *et al.*, 2018). Thus, with the Woodbine and Eagle Ford both being important hydrocarbon-bearing units in the ETB, along with carbon capture utilization and storage (CCUS) potential for these units, a modern sequence stratigraphic framework is especially timely to properly define the plays and play fairways, as well as explain and predict the distribution, thickness variation, and reservoir architecture for the various plays within these units.

1.1 Geologic Background and Previous Work

The ETB (Figure 1) was one of the many Mesozoic sedimentary basins that developed along the southern margin of the North American craton during the Triassic opening of the Gulf of Mexico (Jackson and Seni, 1983). The Jurassic Louann Salt was deposited unconformably on Paleozoic basement rocks and Triassic rift-valley fill in the ETB. Approximately 1500 m (4921') of salt was deposited in the rift valley (Jackson and Seni, 1983). Subsequently, salt diapirism was produced by loading from 1) deposition of a Lower Cretaceous carbonate wedge, 2) progradation of thick Upper Cretaceous siliciclastic units, and 3) uplift, erosion, and tilting of the basin (Jackson and Seni, 1983). However, unlike the Cenozoic succession in the offshore Gulf of Mexico, where fields typically are secondary diapir-related sub-salt structures, in the ETB, many fields are simple salt-cored anticlinal traps (Jackson and Seni, 1983). Adding to the structural complexity, key basement features, such as the San Marcos Arch and Sabine Uplift, were intermittently active into the Late Cretaceous due to Laramide tectonics (Jackson and Seni, 1983). This Laramide compression deformation, and associated uplift and erosion, played a major role in setting up many of the sub-unconformity traps in the ETB, like the super-giant East Texas Field (Jackson and Seni, 1983).

In the late 19th and early 20th century, outcrops of the Cretaceous System across Texas were classically divided into a Lower Cretaceous Comanche Series and an Upper Cretaceous Gulfian Series (Adkins, 1932). With the adoption of the Global Time Scale in the late 20th Century, however, the relative age of the classic Comanche/Gulfian boundary now occurs within the Early Cenomanian. Within the framework of the classic Comanche Series, the sequentially younger, unconformity-bounded, Trinity, Fredericksburg, and Washita Groups were defined (Adkins, 1932). Within the uppermost Washita Group, the Georgetown, Grayson (Del Rio in

South Texas), and Buda Formations were defined from the base up (Adkins, 1932). Sometimes, an additional (younger) unit, termed the "False Buda", also occurs at the top of this succession (Zhang, 2017). In terms of the Washita Group, the Kiamichi and Georgetown Formations are placed within an informal "Lower Washita Subgroup", whereas the Del Rio/Grayson, Buda, and False Buda (where present), are included within an informal "Upper Washita Subgroup".

Within the Gulfian Series, defined the unconformity-bounded Woodbine, Eagle Ford, Austin, Taylor, and Navarro Groups were deposited from the base up (Adkins, 1932). The sandstone-prone strata, at the base of his "Gulfian Series", were originally referred to as the Timber Creek Group (Hill, 1887), a name he subsequently changed to the Woodbine Group (Hill, 1901), when the type locality for this unit was defined near the town of Woodbine, Texas in eastern Cooke County, approximately 60 mi (96.7 km) north of Dallas, Texas. In the Dallas area, the Woodbine was subdivided into its now classic 3-fold lithostratigraphic sub-division, which consists of: 1) a basal (mudstone-prone) Pepper Formation; 2) a middle (sandstone-prone) Dexter Formation; and 3) an upper (lignite- and fossil-bearing) Lewisville Formation (Adkins, 1932). This tri-partite framework was utilized in many subsequent Woodbine subsurface studies (Oliver, 1971; Nichols, Peterson and Wuestner, 1968) in the ETB.

The Eagle Ford Group was defined as the mudstone-prone strata situated between Timber Creek/Woodbine (below) and Austin Chalk (above) (Hill, 1887). The type locality for the Eagle Ford Formation was located on the south bank of the Trinity River in western Dallas County. The Eagle Ford Formation was elevated to group level (Figure 3) based on input from the famed paleontologist W. L. Moremon (Adkins, 1932). The Eagle Ford Group was sub-divided in the Dallas area into the Tarrant, Britton, and Arcadia Park Formations (Adkins, 1932). The basal Tarrant Formation was a thin [15–20' (4.6 – 6.1 m)] fossiliferous unit containing interbedded

sandstone and mudstone. The middle Britton Formation was described as being more mudstone-prone than the basal Tarrant in its basal portions and becoming more interbedded with sandstone in its upper two-thirds. The uppermost Arcadia Park Formation was described as being more mudstone-prone than the directly underlying Britton strata. A Mobil Research borehole in the Dallas area, reported that the Eagle Ford Group was 474' (144.5 m) thick with basal Tarrant Formation, being 20' (6.1 m) thick, the middle Britton Formation being 334' (101.8 m) thick, and the upper Arcadia Park Formation being 120' (36.6 m) thick (Brown and Pierce, 1962). Recently, divided the Britton Formation was sub-divided into 3 members (Figure 3), a basal siliceous Six Flags Member, a middle bentonite-rich Turner Park, and an upper, more sandstone-prone, and less bentonite-prone, Camp Wisdom Member (Denne *et al.*, 2016). Within the Woodbine/Eagle Ford succession in the Dallas area the stratigraphic placement is the Tarrant Formation in the most contentious. The lag at the base of the Tarrant Formation was used to define the base of the Eagle Ford Group in some studies (Adkins, 1932; Adkins and Lozo, 1951; Brown and Pierce, 1962). In contrast, the "Tarrant Beds" were placed within the underlying Woodbine Group (Figure 3) and the base of the Eagle Ford Group was picked at the base of the overlying Britton Formation in other studies (Stephenson, 1952; Clark, 1965; and Denne *et al.*, 2016).

The stratigraphic position assignment of the Tarrant Beds is critical for a variety of reasons. The base of the Tarrant Beds contains the ammonite *Conlinoceras tarrantense*, the faunal (zonal) marker whose first occurrence defines the base of the Middle Cenomanian. Thus, placing the regional base Eagle Ford unconformity, at the base of the Tarrant Beds, restricts the underlying Woodbine Group to the Early Cenomanian. Furthermore, *Conlinoceras tarrantense*, also represents the first (oldest) Upper Cretaceous ammonite species in both the Gulf Coast and Western Interior of the United States (Ogg, Hinnov and Huang 2012). Thus, the occurrence of

this ammonite represents the time when the KWIS was first established and fully connected from the Artic to the north to the Gulf of Mexico to the south.

In contrast to the Dallas area, divided the Eagle Ford Group was subdivided along the outcrop belt from Waco to Austin (Figure 3) into a lower, more carbonate- and bentonite-rich, Lake Waco Formation and an upper, more carbonate- and bentonite-poor, South Bosque Formation (Adkins and Lozo, 1951). A Mobil Research borehole in the Waco area records that the Eagle Ford Group was 199' (60.7 m) thick with basal Lake Waco Formation, being 79' (24.1 m) thick, and the upper South Bosque Formation being 120' (36.6 m) thick (Brown and Pierce, 1962). In this region, also divided the basal Lake Waco Formation was subdivided into three members (Figure 3), named from the base up the: 1) Bluebonnet, 2) Cloice, and 3) Bouldin (Adkins and Lozo, 1951). Within this framework, the middle Cloice Member was noted as being more mudstone-prone and bentonite-rich, and the other two members were descried as intervals dominated by interbedded mudstone and limestone. The Woodbine Group changed in the Waco to Austin region from more sandstone-prone (Dexter) to mudstone-prone (Pepper) facies, as well as thins dramatically, toward the southwest (Adkins and Lozo, 1951). Furthermore, the Woodbine equivalent (Pepper Formation) strata could not be mapped in outcrop "...south or west of the south boundary of Travis County" (Adkins and Lozo, 1951).

In contrast to the ETB in South Texas, where the Woodbine Group equivalent strata are thin to absent, strata between the Buda (below) and the Austin (above) are mapped as the Eagle Ford Group (Figure 3). In this region, a more organic-rich, Lower Eagle Ford Formation (LEF), and more carbonate-rich Upper Eagle Ford Formation (UEF), typically are defined and mapped. The same Eagle Ford Group chrono-stratigraphic framework was established in the outcrops of West Texas (Donovan *et al*., 2012; Donovan, 2014; Donovan *et al.*, 2016) and correlated into the

outcrops and shallow subsurface along the west flank of the ETB (Donovan *et al.,* 2015). The Eagle Ford chronostratigraphic framework (Donovan *et al.,* 2015; Donovan *et al.,* 2019) indicates the base of the UEF occurs within the upper portions of the Lake Waco Formation (Figure 3) in the Waco area and within the Britton Formation (Figure 3) within the Dallas area. Subsequent work (Figure 3) also sub-divided the LEF in the ETB into an organic-rich Lower Member of the Lower Eagle Ford (LM:LEF) and a bentonite-rich Upper Member of the Lower Eagle Ford (UM:LEF) (Donovan and *et al.,* 2019). The UEF in the ETB was defined an argillaceous-rich Lower Member (LM:UEF); a carbonate-rich Middle Member (MM:UEF); and a more argillaceous-rich Upper Member (UM:UEF) (Donovan *et al.,* 2019).

Finally, unlike the outcrop belt along the western margin of the ETB where the base of the Eagle Ford Group was placed above a regional unconformity (Adkins, 1933), in the subsurface a more lithostratigraphic approach was taken (Figure 3). Within this context, a sandstone-prone succession in the southern portion of the ETB was referred to as the Harris Delta within Woodbine Group, even though Oliver (1971) recognized that these sandstone-prone strata were equivalent to the Eagle Ford Group to the west. This lithostratigraphic approach in the subsurface was subsequently followed by Turner and Conger (1984), Berg and Leethem (1985), and Hentz and others (2014). This results in assigning strata to the older Woodbine Group in the subsurface, which are age-equivalent strata assigned to the unconformity-bounded younger Eagle Ford Group along the outcrop belt to the west (Figure 3).

2. RESEARCH PURPOSE AND GOALS

The purpose of this research was to resolve many of the stratigraphic problems associated with the Woodbine and Eagle Ford Groups within the study area. These include:

- Identifying and mapping the regional unconformities that define the 1) base of the Eagle Ford Group; 2) base of the UEF; 3) base of the UM:LEF; 4) base of the MM:UEF; and 5) the base of the UM:UEF across the study areas
- Resolving the proper position assignment of the Tarrant Beds
- Consistently defining and mapping a surface-bounded base to the Lewisville Formation within the Woodbine Group
- Rigorously defining and mapping the various members within the LEF and UEF across the study area
- Properly defining, assigning, and mapping the "Harris Delta", and other reservoir zones within the Woodbine and Eagle Ford Group, so plays and paleogeographic maps can be constructed within a sequence stratigraphic framework, in order to properly explain and predict the presence, distribution, and thickness variations of the reservoirs associated with various conventional and unconventional plays within the ETB.

3. METHODS

3.1 Study Area and Data

This research is located in the northwest portions of the ETB (Figure 2). Unlike previous studies that started in the more sandstone-prone eastern portions of the basin (Hentz, Ambrose and Smith, 2014; Gifford, 2021) and correlated toward the western (mudstone-prone) boundary of the ETB from Dallas to Waco. Key to this research was the inclusion of petrophysical, isotopic ($\delta^{13}C$), and X-ray Fluorescence (XRF) data from two recent USGS shallow boreholes, GC-1 (near Waco), and GC-2 (near Dallas), and well cuttings from 1 industry well, American Liberty Oil Company's Barron 'McClain' 1, to define key sequence stratigraphic surfaces. A grid of 13 regional well-log cross sections (Figure 4) utilized 59 well logs to define and map key sequence stratigraphic boundaries from the outcrop belt into the subsurface. This study utilized XRF data from well cuttings to highlight the utility of using such data to define key geochemical changes associated with critical sequence stratigraphic boundaries across the study area.

3.2 XRF Data Collection

Energy dispersive, high-resolution XRF elemental data was collected using a Bruker Tracer 5i handheld spectrometer for the major [sodium (Na), magnesium (Mg), aluminum (Al), silicon (Si), phosphorus (P), sulfur (S), potassium (K), calcium (Ca), titanium (Ti), manganese (Mn), and iron (Fe)] and trace [vanadium (V), chromium (Cr), barium (Ba), cobalt (Co), nickel (Ni), copper (Cu), zinc (Zn), gallium (Ga), arsenic (As), rubidium (Rb), strontium (Sr), yttrium (Y), zirconium (Zr), niobium (Nb), molybdenum (Mo), lead (Pb), thorium (Th), and uranium (U)] elemental composition of the core and samples (Rowe *et al*., 2012). As outlined on Table I, this elemental data provides insights into; 1) times of terrigenous input into the basin; and 2)

paleogeographic conditions within the water column and seafloor within the ETB during the Cenomanian and Turonian. Stable isotope $\delta^{13}C$ and $d^{18}O$ data from the cores was processed by the Stable Isotope Lab at Texas A&M University. These isotopes provide respective insights into respective stratification and temperatures within the ancient oceans of the world (Grossman, 2012).

Recent work utilizing XRF work on the USGS GC-1 research borehole, located near Waco, established a sub-division of the Eagle Ford Group into an UEF and LEF in the central ETB (Donovan *et al.*, 2019). The UEF also was sub-divided into three distinct unconformity-bounded members, Upper Member (UM:UEF), Middle Member (MM:UEF), Lower Member (LM:UEF). The LEF was sub-divided into two unconformity-bounded members, the Upper Member (UM:LEF) and the Lower Member (LM:LEF).

In this study, a similar approach using isotopic and geochemical (XRF) data was taken to analyze the USGS GC-2, well drilled near Dallas to see if the LEF and UEF and their associated members could also be defined here. A main goal of this study was to determine if the Tarrant Beds strata should be assigned to the older Woodbine Group or younger Eagle Ford Group

Finally, since the GC-2 core in Dallas County spanned only the basal Austin Chalk through the top of the Woodbine Group, cuttings from a nearby well in Ellis county, the Barron 'McClain' 1 (Figure 5) also were analyzed with by XRF to determine the geochemical characteristics of the Woodbine Group and to evaluate if the geochemical-defined chronostratigraphic units defined in the Eagle Ford Group in the GC-2 well could also be delineated with cuttings.

3.3 Preparing Well Cuttings

Cuttings located at the Bureau of Economic Geology (BEG) facility in Austin, were sampled from the Barron 'McClain' 1 well, where the operator collected cutting samples every

10’ (3 m). In this study, the 94 cutting samples spanning from the basal Austin Chalk through the top of the Georgetown Formation were collected for XRF analysis (Figure 5). In this well (Figure 5), over 450’ (137.2 m) of the Eagle Ford Group and just under 400’ (121.9 m) of the Woodbine Group were present for XRF analysis of the cutting samples. The cutting samples were then transported to TAMU and made into pellets suitable for analysis by a Bruker Tracer 5i handheld XRF unit. To make the pellets, the cutting samples were ground up separately in a SPEX 8000 Rock Mixer for 5 minutes. Each sample was sieved to a 90-micron powder and then pressed into a 6 mm thick, 18 mm diameter pellet with a Specac manual hydraulic press. The pellets were then ready be scanned.

3.4 Correlation Methods

Well-log data from MJ systems, the Texas Railroad Commission, and the Texas Water Development Board’s BRACS database was used in this study. The well logs were entered into a Petrel project, a well-log correlation software developed by Schlumberger, as depth calibrated raster images. This program allows users to select wells for a cross section from map view, pick tops, and create maps based on the available geologic data. The elements are also easily manipulated as more new data comes in throughout the study, like changing datums, adding and removing wells from the cross sections, and changing vertical and horizontal scales.

The chronostratigraphic framework of the Woodbine and Eagle Ford Groups in this study is defined by correlating key stratigraphic surfaces: sequence boundaries (sb), maximum flooding surfaces (mfs), and transgressive surfaces (ts). This work follows the surface-based nomenclature (Figure 5) presented in Donovan *et al.* (2015), Donovan *et al.* (2019), and Gifford (2021). Surfaces were named with the letter K (for Cretaceous) and the numbers 1 (older) to 999 (younger). In this study, key surfaces, shown on Figure 5, that were mapped throughout the region are: K720sb for

the base of the Austin Chalk, K630sb for the base of the Eagle Ford Group, and K600sb for the base of the Woodbine Group. The K650sb sub-divides the UEF from the LEF, and also marks the onset of the CTBE (OAE2). The K615ts sub-divides the upper Lewisville Formation from the Lower Dexter Formation in the Woodbine.

Plotting cross sections in Petrel allows the user to easily change datums. Cross sections datumed on the base of the Austin Chalk, the top of the interval of interest, shows the relict basin physiology, whereas datums at the base of the interval of interest, such as the K600sb for the Eagle Ford and Woodbine or the K650sb focus on the Harris Delta, are better for seeing stratal terminations.

4. RESULTS

4.1 Geochemical (XRF), Isotopic, and Petrophysical Learnings from Cores and Cuttings

4.1.1 Overview

The USGS GC-1 research borehole (Figure 6) is located southwest of Waco (31.4867/-97.2474), near the classic Cloice Branch locality studied by Adkins and Lozo (1951). The USGS GC-2 research borehole (Figure 7) is located in south Dallas (32.6917/-96.8922) near the old settlement of Eagle Ford the type locality for the Eagle Ford Group. The borehole is located near the Eagle Ford localities visited by Jacob *et al.* (2013) on a GSA Fieldtrip, as well as outcrops studied by Kennedy (1988) for his classic ammonite work on the Eagle Ford Group. Petrophysical data for the USGS GC-2 was not collected for the bottom of the core due to borehole problems encountered during logging, but a core-gamma-ray log of this interval which spans the UM:LEF to the uppermost Woodbine Group, was collected and is plotted on Figure 7 along with the petrophysical, isotope, TOC, and XRF data. In terms of their locations and cored intervals, the GC-1 and GC-2 are essentially twins of the Mobil Research Boreholes drilled in the late 1950's (Brown and Piece, 1962). Unfortunately, the Mobil cores no longer exist and no petrophysical data was ever published for them.

The American Liberty Barron 'McClain' 1 well (Figure 8), whose cuttings were studied as part of this research, is located in the northeast part of Ellis County (32.465/-96.619), about 21 miles southeast of the GC-2. XRF results were collected on all three locations samples. However, TOC and $\delta^{13}C$ isotope data are only available for the USGS research boreholes.

4.1.2 Surface Characteristics

The K580sb, which marks the base of the Grayson Formation, and the top of the Georgetown, occurs in the Barron 'McClain' 1 well (Figure 8). In this well, the K580sb is marked by a sharp (upward) drop in SP and resistivity values, and geochemically by gradual decreases in Ca content, but gradual increases in Al, Si, Ti, Fe, Mn, Ni, Sr, V, and P content.

In most of the subsurface study area, the base of the Woodbine Group (K600sb) overlies the Early Cenomanian Buda Formation. However, in the shallow subsurface along the outcrop belt, the locations of all three XRF datasets, the Woodbine Group was deposited unconformably on the Early Cenomanian Grayson Formation, because the Buda Formation was eroded. The K600sb, which marks the base of the Woodbine Group, occurs in the GC-1 (Figure 6) and the Barron 'McClain' 1 well (Figure 8). In the GC-1 borehole (Figure 8), this surface is petrophysically marked by a subtle (upward) decrease in GR and resistivity values, and geochemically marked by more distinct (upward) decreases in Ca and Sr content, and increases in Al, Fe, Ni content. Similar changes also occur at the interpreted K600sb in the Barron 'McClain' 1 well (Figure 8), along with more distinct (upward) increases in Si and Ti content.

The K615ts defines the base of the Lewisville Formation in this study. Regionally, this surface marks the change from higher net/gross fluvial deposits (below) to lower net/gross fluvial deposits above. Although there is very little difference in the Dexter and Lewisville Formations geochemically, the McClain #1 well shows a drop in Al and V and a positive spike in Fe and Mn at the K615ts (Figure 8).

The K630sb marks the interpreted base of the Eagle Ford Group in this study. This surface, and the overlying K630 sequence (LM:LEF) occurs in the GC-2 and the Barron 'McClain' 1

(Figure 8) but is interpreted to be absent in the GC-1 (Figure 6), where the younger K640sb is interpreted to unconformably overlie the Woodbine Group. In the GC-2 core (Figure 7), the K630sb marks the boundary between un-fossiliferous, TOC- and Ca-poor Woodbine Group strata below, from fossiliferous TOC- and Ca-bearing strata (above) of the classic Tarrant Member of the Eagle Ford Group. In the core GR log for the GC-2 a distinct GR drop is associated with the strata above the basal limestone bed in this unit (Figure 7). In the core photos of this boundary (Figure 9), distinct cobble-sized rip-up clasts overlie this contact. Adjacent outcrop work (Kennedy, 1988) places the first occurrence of the ammonite zonal marker *Conlinoceras tarrantense*, whose first occurrence defies the base of the Middle Cenomanian, in the basal beds of the Tarrant Member. As noted previously, this zonal marker represents the first (oldest) Upper Cretaceous ammonite species in both the Gulf Coast and KWIS (Ogg, Hinnov and Huang, 2012), thus marking the time that the KWIS became fully established and connected from the Artic to the north to the Gulf of Mexico to the south.

The K640sb marks the base of the UM:LEF in this study. This surface, and the overlying K640 sequence (UM:LEF) occurs in all three wells where we have XRF data. In the GC-1, the K640sb directly overlies the Woodbine Group (Figure 6). In this well (Figure 6), crossing this surface upward is marked by a GR decrease and resistivity increase, as well as a sharp increase in TOC, Ca, Fe. Mo, Ni, and V; and abrupt decrease in Al, Si, Fe, content occurs. In GC-2 (Figure 7) and #1 McClain (Figure 8), similar petrophysical and geochemical changes also occur upward across this boundary.

The K650sb marks the base of the UEF throughout the study area, and this surface is overlain by the LM:UEF. Petrophysically, in all three wells (Figures 6-8), a sharp upward drop in GR values occurs across this boundary. Geochemically, all three wells (Figures 6-8) record an

upward drop in TOC, Al, Si, Fe, Mo, Ni, and V content. However, most importantly, in the GC-1 and GC-2 boreholes (Figures 6 and 7), where $\delta^{13}C$ data was obtained, the K650sb marks the onset of the positive $\delta^{13}C$ isotope excursion associated with the onset of the CTBE (OAE2).

The K670sb marks the base of the MM:UEF in this study. As illustrated in Figures 6 and 7, this surface marks the unconformable termination of the CTBE (OAE2). Above this boundary, a higher-resistivity, organic and Ca-rich succession (MM:UEF) occurs (Figures 6 and 7). The distinct increase in resistivity that marks the base of this unit was used to define it where core control is absent. Based on the XRF data from the cuttings in the #1 McClain, the increased carbonate content in this interval also is responsible for the increased resistivity (Figure 8). The K670sb coincides with the base of the classic Arcadia Park Formation in Dallas area outcrops (Figure 7).

The K700sb defined in this study marks the base of the UM:UEF. Based on the geochemical data in the GC-1 (Figure 6) and GC-2 (Figure 7), this boundary marks a change from more organic- and carbonate-rich strata below, to more organic- and carbonate-poor, as well as Al- and Si-enriched strata above.

The K720sb marks the base of the Austin Chalk in this study. In all three wells (Figures 6-8), the base of the Austin Chalk is marked by a sharp (upward) drop in GR values and increase in resistivity values. Geochemically the base of the Austin Chalk (Figures 6-8) is characterized by an increase in Ca-content and decrease in Al- and Si-content.

4.1.3 Sequence Characteristics

The strata situated between the K600sb and the K630sb, corresponds to the Woodbine Group and consists of TOC- and Ca-poor, as well as Al, Si, Ti, and Fe-enriched strata (Figures 6

and 8). The database in this study is limited, but no clear discernable geochemical differences appear to occur between the mudstone from the Pepper, Dexter, and Lewisville shales.

The K630 Sequence, or the LM:LEF, occurs in the GC-2 (Figure 7) and the McClain #1 (Figure 8). It also corresponds to the classic Tarrant Beds of Adkins (1932) and Adkins and Lozo (1951). Petrophysically, this sequence is unique, in that it has as a high-GR and low SP/Resistivity zone that is recorded between the Woodbine Group strata below and the UM:LEF above (Figures 7 and 8). Geochemically, the LM:LEF appears somewhat transitional at first glance, in that, like the underlying Woodbine it is Al, Si, and Ti-enriched (Figure 7). However, its base also marks the onset of Ca- and TOC-enriched strata typical of the LEF. In core, the basal Eagle Ford Group is more obvious (Figure 9) as a distinct cobble lag marks its base, and the overlying units consist of interbedded fossiliferous mudstone, sandstone, and limestone, and are distinctly different from the underlying interbedded un-fossiliferous mudstone and sandstone of the underlying Woodbine Group (Figure 9).

The K640 Sequence, or the UM:LEF, is an Ca- and TOC- rich sequence consisting in core of interbedded carbonate mudstone, limestone, and abundant bentonite. On geophysical logs (Figures 6-8), it is characterized as a zone of elevated GR and resistivity values, likely driven by its abundant TOC and bentonite content. In the Dallas area, this sequence corresponds to strata typically assigned to the Turner Park Member of the Britton Formation (Figure 7).

The K650 Sequence, or the LM:UEF, is a TOC- and Ca-poor and Al, Si, , and Fe-enriched sequence. A sharp GR drop marks it base and this boundary also marks the base of the UEF. In the Dallas area, this sequence corresponds to the traditional Camp Wisdom Member of the Britton Formation (Figure 7). The most distinctive characteristic of the LM:UEF, based on the GC-1 and GC-2 cores (Figures 6 and 7), is that this sequence coincides with the positive $\delta^{13}C$ isotope

excursion, typically associated with the CTBE (OAE2). Interestingly, this sequence is 230' (70 m) thick in the GC-2 (Figure 7), but only 12' (3.7 m) in the GC-1 (Figure 6).

The K670 Sequence, or the MM:UEF, was first proposed by Donovan *et al.* (2019), but this research more clearly defines and characterizes this unit. In the GC-1 and GC-2 boreholes (Figures 6 and 7), the MM:UEF is characterized as a Ca- and TOC-enriched sequence with elevated resistivity values, when compared to the underlying LM:UEF. In both the GC-1 and GC-2 cores (Figure 6 and 7), the base of this sequence marks the top of the positive $\delta^{13}C$ isotope excursion associated with the CTBE (OAE2). In the Dallas area (Figure 7), the basal boundary also coincides with the base of the Arcadia Park Formation (Adkins, 1983; Kennedy, 1988). Based on his ammonite work on the Eagle Ford Group outcrops around Dallas, Kennedy (1988) interpreted a major hiatal break at the base of this unit.

The K700sb, or the base of the UM:UEF, is defined as a TOC- and Ca-poor, and Al-, and Si-enriched succession at the top of the Eagle Ford Group within the study area (Figures 6-8). Petrophysically, it is a low SP/resistivity zone with elevated GR values, when GR logs are available (Figures 6-8).

Finally, the Austin Chalk is a Ca- and Sr-enriched, as well as a low Al-, Si, and Fe-sequence that was deposited unconformably above the Eagle Ford Group (Figures 6-8). Petrophysically, the K720sb, which marks its base, is denoted by a sharp (upward) drop in GR and SP values, and increase in resistivity (Figures 6-8).

4.2 Cross Sections and Geologic Maps

4.2.1 Cross Section Overview

The surfaces and sequences defined in the GC-1 (Figure 6), GC-2 (Figure 7), and Barron 'McClain' 1 (Figure 8) from their lithological, petrophysical, and geochemical characteristics were tied into a grid of six north to south cross section lines, and seven west to east cross section lines, that included 59 different wells. Cross-section NS-Regional 1 (Figures 10a and 10b) is shown to illustrate the North to South variations of the units, whereas cross-section EW-Regional 1 (Figure 11a and 11b) shows the West to East variations. Both cross sections are datumed on the base of the Austin Chalk (Figures 10a and 11a) and on the base of the Woodbine Group (10b and 11b).

4.2.2 Cross Section Observations

EW-Regional 1 (Figure 11a and 11b) indicates the sequential westerly truncation (thinning) of the Buda and Grayson Formations, beneath the K600sb, the westerly truncation (thinning) of the Woodbine Group (Lewisville) beneath the K630sb, and the easterly truncation (thinning) of the LEF beneath the K650sb at the base of the UEF. On this cross section, the members of the UEF change little.

NS-Regional 1 (Figures 10A and 10B) revealed similar relationships. This cross section also highlights the sequential northerly truncation (thinning) of the Buda and Grayson Formations, beneath the K600sb, the southern truncation (thinning) of the Woodbine Group (Lewisville) beneath the K630sb, and the northerly truncation (thinning) of the LEF beneath the K650sb at the base of the UEF. When hung on the base of the Austin Chalk (Figure 10a), NS-Regional 1 highlights that the thickest accumulations of both Eagle Ford and Woodbine Groups strata occur in the northern portions of Van Zandt County.

4.2.3 Map Overview

Based on the correlations of this study, a variety of isochore, structure contour, and facies maps were constructed. On the isochore and facies map, the Mexia-Talco fault zone and Louann Salt domes, as mapped in Jackson and Seni (1984), are highlighted since these features may explain various inconsistencies in unit thickness and sub-sea elevations.

Structure contour maps for the: 1) the K600sb/base of the Woodbine Group (Figure 12A), 2) K650sb/base of the UEF (Figure 12B), and K720sb/base of the Austin (Figure 12C) were constructed. Isochore maps for the 1) Buda Formation (Figure 13A) , 2) Pepper and Dexter (Figure 14A), 3) Lewisville Formation (Figure 15A), 4) Total Woodbine Group (Figure 13B), 5) the LEF (Figure 16A), 6) the UEF (Figure 16B), and 7) the three UEF members (Figure 17) were also constructed. Facies maps of the 1) Dexter Formation (Figure 14B), 2) Lewisville Formations (Figure 15B), and 3) LM:UEF/Harris Delta (Figure 18) also were generated.

4.2.4 Map Observations

The Buda Formation isochore map (Figure 13A) indicates gradually thickening to the east. Areas where the Buda Formation is absent (Figure 13A) occurs structurally updip of the Mexia-Talco fault zone. The Upper Woodbine (Lewisville Formation) isochore map (Figure 13B) shows the thickest part of this unit to the northeast and thinning to 0 thickness to the southwest. The Dexter Formation (Figure 14A) also is thickest to the northeast and thins to the southwest but it occurs throughout the study area. Total Woodbine Group thickness (Figure 13C) ranges from almost 900’ (274.32 m) to the east to less than 60’ (18.3 m) thick in the southwest, toward the GC-1 well.

The LEF isochore (Figure 16A) shows the thickest accumulation [>60’ (18.3 m)] to the south and thinning to zero to the north (Hunt County) and to the east (Wood and Smith Counties). The LM:UEF (Figure 17A) resumes the trend in the Woodbine formations with the thickest accumulations of almost 300’ (91.4 m) to the northeast and thinning to the southwest. The MM:UEF (Figure 17B) is similar with a little over 200’ (61 m) thickness to the northeast and less than 50’ (15.2 m) in the south. There is not as much variation in the thickness of the UM:UEF (Figure 17C) with a range from ~70’ (21.3 m) to under 20’ (6.1 m) along the outcrop belt.

All the structure contour maps (Figure 12) follow the same trend, with all units being exposed in the Middle Cretaceous outcrop belt, and all dipping to the southeast. The angle of contour lines with decreasing depth also are parallel with the Mexia-Talco fault zone. These structure contour maps were generated in the Petrel and bullseye features in the maps coincide with the locations of the Louann Salt domes.

Comparing the Lewisville Formation (Figure 15B) and Dexter Formation (Figure 14B) facies maps, the Dexter Formation has a higher volume of sand overall, with over 75% of the succession being interpreted as sand in the northeast part of the study area. Both are sandiest to the northeast and the amount of sand decreases to the southwest.

The facies map of the LM:UEF, which is coeval to the Harris Delta, was combined (Figure 18) with the facies map of the Harris Delta from Gifford (2021) to the south. Orange represents areas with more than 50% of the sequence being sand. The areas colored yellow represent regions where the sequences are less than 50% sand. The areas colored gray are interpreted to be mudstone-dominated (less than 10% sand). Overall, the LM:UEF sequence becomes more mudstone-prone to the west and south (Figure 18). This work expands the sandstone play fairway established in Gifford (2021) to the northeast of this study area.

5. DISCUSSION

5.1 Buda Formation and Woodbine Group Play Fairways

Structure contour maps (Figure 12) of the base Woodbine Group, base UEF, and base Austin Chalk illustrate similar trends: the ETB strata here dips to the east, as well as to the south, with the deepest portions of the basin in the southwest portions of the study area.

The K600sb that marks the base of the Woodbine Group shows angular discordance, that sequentially bevels, and then truncates, the Buda Formation to the north and west (Figures 10A and 11A). The isopach map of the Buda Formation (Figure 14A) shows that this unit is over 75' (22.9 m) thick to the west and thins to zero to the northwest. The zero edge of the Buda Formation (Figure 14A) marks the structurally updip limit of any Buda Formation plays within the basin.

Within the study area, the Woodbine Group overlies the K600sb (Figure 5). As illustrated on Figure 13B, the total Woodbine Group varies in thickness from over 900' (274.3 m) to the west to less than 300' (91.4 m) to the east. In this study, a regional surface, the K615ts, was identified and mapped within the Woodbine Group (Figures 10 and 11), This surface was used to separate more sandstone-prone strata of the Dexter Formation (below) from the more mudstone-prone Lewisville Formation (above). As illustrated on Figures 14A and 14B, the Dexter Formation ranges in thickness from over 400' (121.9 m) to the east to below 100' (30.5 m) in the southwest, and becomes increasingly mudstone-dominated to the southwest. As defined and mapped in this study, the overlying Lewisville Formation (Figure 15A) is over 300' (91.4 m) thick in the eastern portions of the study area, but thins to the southwest through Ellis, Navarro, and Freestone Counties, due to interpreted regional truncation by the unconformity (K630sb) at the base of the

overlying Eagle Ford Group (Figures 10A and 11A). Similar to the Dexter Formation, the Lewisville Formation becomes mudstone-dominated to the south and west (Figure 15B).

5.2 Lower Eagle Ford Formation and "Tarrant Beds" Assignment

In the Dallas area, the K630sb marks the base of the Eagle Ford Group and is placed at the base of the "Tarrant Beds". This unconformity displays distinct angular discordance and appears to mark a distinct break in the depositional fabric in the basin based on the distribution of the strata below and above the angular discordance (Figures 11A and 11B). As discussed previously, the overlying LM:LEF is petrophysically distinct, and can be mapped as a high GR, low (+) SP, and low resistivity zone regionally (Figure 5). Geochemically, while siliciclastic-rich like the underlying Woodbine Group, the LM:LEF can be differentiated by the onset of TOC, Ca, and Mo content (Figure 7). Most importantly, the basal K630sb (Figure 9) also marks the change from un-fossiliferous (Woodbine) mudstone and sandstone below to fossiliferous marine strata of Eagle Ford Group above. Furthermore, a distinct cobble bed marks its base in the GC-2 core (Figure 9). In the LM:LEF, the ammonite fauna contained within the basal portions of this unit are the oldest Tethyan species also in the KWIS marking the time that the seaway first became established. Unlike the underlying Woodbine Group, fauna and flora in the Eagle Ford Group also are age equivalent to (Graneros and Greenhorn) strata in the KWIS (Cobban and Scott, 1972).

The K640sb marks the base of the UM:LEF. The UM:LEF is an organic-, uranium-, carbonate, and bentonite-rich sequence deposited above the LM:LEF in the GC-2 core near Dallas (Figure 7). However, in the GC-1 core (Figure 6) near Waco, organic-, uranium-, carbonate-, and bentonite-rich strata were deposited directly on the Woodbine (Pepper Formation). This data suggests that the stratigraphically older LM:LEF defined in Dallas does not occur in the Waco area, likely truncated by the K640sb at the base of the UM:LEF. This interpretation is supported

by the biostratigraphy of Adkins and Lozo (1951), Kennedy and Cobban (1990), and Denne et al. (2016), who all concluded that the basal Eagle Ford strata in the Waco area were younger than the "Tarrant Beds" of the Dallas area. This new interpretation differs from previous work of Donovan *et al.* (2015), and Donovan *et al.* (2019), who correlated the LM:LEF into the Waco area. The XRF geochemical work in the GC-1 (Figure 6), as well as the biostratigraphy, clearly does not support strata equivalent to the Tarrant Beds (LM:LEF) being in the GC-1 core or the Waco area.

The K650sb marks the top of the LEF. Using the K630sb, or when absent the K640sb, as the base of the LEF, and the K650sb as the top of the LEF, the LEF was mapped across the study area (Figures 10 and 11). Based on the regional cross section grid , an isopach map of the LEF (Figure 16A), indicates that the organic-rich mudstone of the LEF varies from >60' (18.3 m) in the southwest portions of the study area, but thins, and eventually is truncated to the north (Rains County) and to east (Wood and Smith Counties) by the K650sb, at the base of the overlying UEF. This truncation edge (Figure 16A) marks the northern and eastern limits of any LEF unconventional reservoir play. Using the K720sb at the base of the Austin Group, isopach maps of the total Eagle Ford Group (Figure 13A) and UEF Formation (Figure 16A) were made. These maps indicate similar trends at >500' (152.4 m) to the northeast and thinning to under 300' (91.4 m) (total Eagle Ford Group) and 200' (61 m) (UEF) to the southwest.

5.3 Upper Eagle Ford Formation and the Cenomanian/Turonian Boundary Event

In this study, the K650sb also marks the base of the UEF. A distinct GR and resistivity drop characterizes the K650sb throughout the study area (Figures 6-8). Throughout most of the study area (Figure 6-8) this surface separates more organic-, uranium, and carbonate-rich LEF strata (below) from more organic- and uranium-poor, and argillaceous-rich, UEF strata (above). This boundary (Table I) thus marks a major change from more anoxic sea-floor conditions, associated

with restricted sea-way column circulation patterns (below), to more oxic sea-floor (epicontinental seaway) conditions, associated with an open sea-way column circulation patterns (above).

Isotope work on the USGS GC-1 (Figure 6) and GC-2 (Figure 7) boreholes, near Waco and Dallas respectively, indicate that the onset of the positive ($\delta^{13}C$) carbonate isotope excursion associated with the CTBE (OAE2), also coincides with the K650sb at the base of the UEF Formation. This geochemical event provides an additional proxy to define the base of the UEF within the study area.

A regional unconformity, the K670 marks the top of the Lower Member of UEF (LM:UEF) as defined in this study. This surface (Figures 6 and 7) also coincides with the termination of the positive ($\delta^{13}C$) carbonate isotope excursion associated with the CTBE. The K670sb (Figure 7) corresponds to the classic boundary to define the Britton/Arcadia Park contact in the Dallas area (Kennedy, 1984; Denne *et al.*, 2016). In terms of the LM:UEF it equates to Denne and others (2016) Camp Wisdom Member of the Britton Formation (Figure 7). The unconformity-bounded LM:UEF varies from 230' (70.1 m) in the GC-2 borehole to less than 12' (3.7 m) thick in the GC-1 borehole. Thus, the geochemical and isotopic data in the GC-2 (Figure 7) documents the presence of a major siliciclastic depocenter during the Latest Cenomanian in the northern portion of the ETB. What makes the LM:UEF and its thickness in the GC-2 well even more remarkable is that based on outcrop ammonite work by Kennedy (1988) in the Dallas area, the thick siliciclastic-rich (Upper Britton) strata represents just the earliest portion of the CTBE , spanning only the (*Sciponoceras gracile)* ammonite zone, which occurs at the onset (base) of the CTBE in the Late Cenomanian (Ogg, Hinnov and Huang, 2012).

5.4 Harris Delta Sandstone-play Fairway

Regional correlations of this study, also indicate that the LM:UEF is coeval to the classic Harris Delta System in the southern portions of the ETB (Figure 18). Paleogeographic maps of the LM:UEF in this study suggest that the sandstone-play fairway way associated with the Harris Delta System has more regional extent than previously reported (Oliver, 1971; Gifford, 2021).

The thickness variations associated with the unconformity-bounded LM:UEF, which also coincides with positive ($\delta^{13}C$) carbonate isotope excursion associated with the CTBE, is inciteful. The recognition of this unit, and its bounding surfaces, provides valuable insights into explaining and predicting the distribution and thickness variations of the CTBE (OAE2), in the ETB, across Texas, and elsewhere. The interpreted unconformity at its base, as well the associated siliciclastic input in this study area, may also provide additional insights into the driving mechanisms associated with the CTBE (OAE2), as well as the seafloor changes from more anoxic to less anoxic conditions that occur at its base of the CTBE in Texas, as well as in the KWIS (Ma *et al.*, 2014).

Finally, the unconformities, within the Eagle Ford Group, suggest that in mudstone-prone successions within shallow epicontinental seaways, any attempt to define astronomically calibrated cycles (Ma *et al.*, 2014), as well as sedimentation rates may be fraught with peril, if the major hiatal breaks. are not identified, mapped, and accounted for during astronomical analyses. The stratigraphic record consists of 3 components: 1) what was deposited, 2) what was eroded, and 3) what is preserved. The erosional and preserved components of the stratigraphic record are not commonly considered in studies of mudstone-prone successions within shallow epicontinental seaways like the Eagle Ford Group.

6. CONCLUSIONS

This research indicates the utility of integrating petrophysical, isotopic, and geochemical (XRF) data from research cores along the basin margin in to help: 1) define sequence boundaries, 2) identify and correlate unique chronostratigraphic units, and 3) correlate the defined sequence boundaries and sequences into the deeper subsurface in order to define plays, as well as explain and predict reservoir distributions within the Woodbine and Eagle Ford Groups within the ETB. Of particular importance in this study was finding that XRF analyses on cuttings could also be used to help define the surfaces and depositional sequences.

Important stratigraphic surfaces defined in this study are the K600sb, K615ts, K630sb, K640sb, K650sb, and the K670sb. The K600sb marks the base of the Woodbine group and controls the limit of play fairways associated with the Buda Formation by sequentially beveling and truncating it to the west. The K615ts divides the Woodbine Group into the more sandstone-prone Dexter Formation (below) from the more mudstone-prone Lewisville Formation (above). Both formations become increasingly mudstone prone to the southwest. The Dexter Formation ranges in thickness from over 400’ (121.9 m) to the east to < 100’ (30.5 m) in the southwest. The Lewisville Formation is >300’ (91.4 m) thickness to the east but is truncated by the K630sb to the southwest.

The K630sb divides the un-fossiliferous mudstones and sandstones of the Woodbine Group below from the fossiliferous marine strata of Eagle Ford Group above. This boundary is observed the base of the Tarrant Beds as both a change in depositional fabric and a faunal (zonal) marker in the GC-2 core. The K640sb marks the base of the organic-, uranium-, and carbonate-rich UM:LEF and truncates the underlying LM:LEF in the Waco area. The K650sb is characterized by a distinct GR and resistivity drop and indicates the top of the organic-rich

mudstones of the LEF. The LEF is >60’ (18.3 m) in the Waco area but thins and get truncated by the K650sb to the north and east. The transition from more organic-, uranium-, and carbonate-rich LEF strata (below) to more organic- and uranium-poor, and argillaceous-rich, UEF strata (above) marks a major change from anoxic to more oxic sea-floor conditions associated with an open sea-way column circulation pattern.

Geochemical and isotopic analysis revealed that the K650sb also corresponds to the onset of the positive ($\delta^{13}C$) carbonate isotope excursion associated with the CTBE, which is also commonly termed the OAE2. The LM:LEF, between the K650sb and K670sb, contains a major clastic depocenter during the Latest Cenomanian in the northern portions of the ETB that is coeval to the classic Harris Delta System from the southern portions of the ETB. This paleogeographic map of the LM:LEF from this work suggests the sandstone-play fairway way associated with the Harris Delta System has more regional extent than previously reported.

In the past, erosional and preserved components of the stratigraphic record were not commonly considered in studies of mudstone-prone successions within shallow epicontinental seaways like the Eagle Ford Group. However, ruinous inconsistencies occur if the major hiatal breaks are not identified, mapped, and accounted for. Recognizing the correlation between the CTBE (OAE2) and the LM:LEF by its bounding surfaces, may provide additional insights into the driving mechanisms associated with the CTBE (OAE2).

REFERENCES

Algeo, T. J., and Rowe, H. D., 2012, Paleoceanographic applications of trace-metal concentration data: Chemical Geology, v. 324, p. 6-18.

Adkins, W. S., and F. E. Lozo, 1951, Stratigraphy of the Woodbine and Eagle Ford, Waco Area, Texas: Fondren Science Series, p. 101–161.

Adkins, W. S., E. H. Sellards, and F. B. Plumber, 1932, The Mesozoic systems in Texas, Part 2, in The Geology of Texas: University of Texas Bulletin, 3232, 239–518 p.

Banner, J. L., 1995, Application of the trace-element and isotope geochemistry of strontium to studies of carbonate diagenesis: Sedimentology, v. 42, p. 805-824.

Berg, R. B., and J. T. Leethem, 1985, Origin of Woodbine-Eagle ford Reservoir Facies, Kurten Field, Brazos County, Texas: Gulf Coast Association of Geological Societies Transactions, v.35, p. 11-18

Blakey, R., 2019. Global Paleogeography. Global Series: Cretaceous.

Brown, C. W., and R. L. Pierce, 1962, Palynologic Correlations in Cretaceous Eagle Ford Group, Northeast Texas: AAPG Bulletin, v. 46, no. 12, p. 2133–2147.

Brumsack, H. J., 2006, The trace metal content of recent organic carbon-rich sediments: Implications for Cretaceous black shale formation: Palaeogeography, Palaeoclimatology, Palaeoecology, v. 232, p. 334-361.

Calvert, S. E. and Pedersen, T. F., 1993, Geochemistry of Recent oxic and anoxic marine sediments: Implications for the geological record. In: R.J. Parkes, P. Westbroek and J.W. de Leeuw (Editors), Marine Sediments, Burial, Pore Water Chemistry, Microbiology and Diagenesis. Mar. Geol., v. 113, p. 67-88.

Clark, D. L., 1965, Heteromorph ammonoids from the Albian and Cenomanian of Texas and adjacent areas: Mem. geol. Soc. Am., v. 95, 24 p.

Cobban, W.A. and Scott, G. R., 1972. Stratigraphy and ammonite fauna of the Graneros Shale and Greenhorn Limestone near Pueblo, Colorado.

Denne, R. et al., 2016, Biostratigraphic and Geochemical Constraints on the Stratigraphy and Depositional Environments of the Eagle Ford and Woodbine Groups of Texas: AAPG Memoir, v. 110, p. 1–86, doi:10.1306/13541957M1103660.

Donovan, A. D., S. Gifford, A. Pramudito, M. Meyer, M. C. Pope, and S. Paxton, 2019, Unraveling the secrets of the Eaglebine: SEG Global Meeting Abstracts, p. 836-849, doi:10.15530/urtec-2019-1028.

Donovan, A. D., Staerker, T. S., Gardner, R., Pope, M. C., Pramudito, A., Wehner, M., 2016, Findings from the Eagle Ford Outcrops of West Texas and Implications to the Subsurface of South Texas, in J. A. Breyer, ed., The Eagle Ford Shale: A renaissance in U.S. oil production: AAPG Memoir 110, p. 301–336.

Donovan, A. D., Staerker, T. S., Gardner, R., Pramudito, A.,, 2015, Chronostratigraphic relationships of the Woodbine and Eagle Ford groups across Texas: Gulf Coast Association Geological Societies Transactions, v. 4, p. 67–87.

Donovan, A.D., 2014, A Sequence Stratigraphic Framework for Defining and Differentiating the Woodbine & Eagle Ford Groups across Texas: Abstract AAPG Annual Meeting Houston, April 2014

Donovan, A.D., T.S. Staerker, A. Pramudito, W. Li, M.J. Corbett, C.M. Lowery, A.M. Romero, and R.D. Gardner, 2012, The Eagle Ford Outcrops of West Texas: A Field Laboratory for Understanding Heterogeneities Within Unconventional Mudstone Reservoirs, GCAGS Journal, v1. p.162-185.

Gifford, S., 2021, The Sequence Stratigraphy of The Woodbine and Eagle Ford Groups in The East Texas Basin (USA): A New Chronostratigraphic Framework to Properly Identify and Map Their Associated Plays and Play Fairways [master's thesis]: Texas A&M University, College Station, Texas, 117 p.

Grossman, E. L., 2012, Applying oxygen isotope paleothermometry in deep time. The Paleontological Society Papers, 18, 39-68.

Halbouty, M. T., 1991, East Texas Field, U.S.A., AAPG Special Publication A024: Stratigraphic Traps II, p.189-206.

Hentz, T. F., Ambrose, W. A., and Smith, D. C., 2014, Eaglebine play of the southwestern East Texas basin: Stratigraphic and depositional framework of the Upper Cretaceous (Cenomanian–Turonian) Woodbine and Eagle Ford Groups: AAPG Bulletin, v. 98, no. 12, p. 2551–2580, doi:10.1306/07071413232.

Hill, R. T., 1901, Geography and geology of the Black and Grand prairies, Texas: U.S. Geological Society 21st Annual Report, pt. 7, 666 p

Hill, R. T., 1887, The topography and geology of the Cross Timbers and surrounding regions in northern Texas: American Journal of Science, 3rd series, v. 33, p. 291–303.

Jackson, M. L. W., and Laubach, S. E., 1991, Structural History and Origin of the Sabine Arch, East Texas and Northwest Louisiana: The University of Texas at Austin, Bureau of Economic Geology, Geological Circular 91-3, 47 p.

Jackson, M. P. A., and S. J. Seni, 1983, Geometry and evolution of salt structures in a marginal rift basin of the Gulf of Mexico, east Texas: Geology, v. 11, no. 3, p.131–135.

Jacobs, L.L., M.J. Polcyn, D., Winkler, D.A., Myers, T.S., Kennedy, J.G., and Wagner, J.B., 2013, Late Cretaceous strata and vertebrate fossils of North Texas, in Hunt, B.B., and Catlos, E.J., eds., Late Cretaceous to Quaternary Strata and Fossils of Texas: Field Excursions Celebrating 125 Years of GSA and Texas Geology, GSA South-Central Section Meeting, Austin, Texas, April 2013: Geological Society of America Field Guide 30, p. 1–13.

Kaufman, E.G., 1995, Global Change Leading to Biodiversity Crisis in a Greenhouse World: The Cenomanian- Turonian (Cretaceous) Mass Extinction, in National Academy of

Sciences: National Research Council Studies in Geophysics, Effects of Past Global Change of Life, p.47-71.

Kennedy, W. J., 1988, Late Cenomanian and Turonian ammonite faunas from north-east and central Texas: Special Papers in Paleontology, v. 39, p. 131.

Ma, C., Meyers, S.R., Sageman, B.B., Singer, B.S. and Jicha, B.R., 2014. Testing the astronomical time scale for oceanic anoxic event 2, and its extension into Cenomanian strata of the Western Interior Basin (USA). Bulletin, 126(7-8), pp.974-989.

McCreary, M., 2022, Chemostratigraphic and Sequence Stratigraphic Analysis of the Austin Chalk in the Outcrops and Subsurface of Texas: [master's thesis] Texas A&M University, College Station, Texas, 43 p

McNulty Jr, C., 1954, Fish bed conglomerate and sub-Clarksville sand, Grayson and Fannin counties, Texas: AAPG Bulletin, v. 38, no. 2, p. 335-337.

McNulty Jr, C., 1966, Nomenclature of uppermost Eagle Ford Formation in northeastern Texas: AAPG Bulletin, v. 50, no. 2, p. 375-379.

Meyer, M. J., 2018, High-resolution chemostratigraphy of the Woodbine and Eagle Ford Groups, Brazos Basin, Texas, master's thesis, Texas A&M University, College Station, Texas, 68 p.

Meyer, M. J., A. D. Donovan, and M. C. Pope, 2020, in press, Depositional environment and source rock quality of the Woodbine and Eagle Ford Groups, southern East Texas (Brazos) Basin: An integrated geochemical, sequence stratigraphic, and petrographic approach: AAPG Bulletin.

Nichols P. H., Peterson G. E., Wuestner C. E., 1968. Summary of Subsurface Geology of Northeast Texas: Natural Gases of North America, v. 1- 2

Ogg, J., Hinnov, L.A. and Huang, C., 2012, Cretaceous. doi:10.1016/B978-0-444-59425-9.00027-5.

Oliver, W. B., 1971, Depositional Systems in the Woodbine Formation (Upper Cretaceous), Northeast Texas, 73: The University of Texas at Austin, Report of Investigations, 30 p.

Pearce, T., and I. Jarvis, 1992, Applications of geochemical data to modelling sediment dispersal patterns in distal turbidites- Late Quaternary of the Madeira abyssal plain: Journal of Sedimentary Petrology, v. 62, p. 1112–1129.

Raiswell, R., and Canfield, D. E., 1998, Sources of iron for pyrite formation in marine sediments: American Journal of Science, v. 298 (3), p. 219-245.

Renard, M., 1979, Aspect géochimique de la diagenèse des carbonates. Teneurs en strontium et en magnésium des carbonates: essai d'interprétation de l'inversion de la corrélation SrMg observée dans les carbonates du domaine pélagique par rapport à ceux du domaine néritique. Bull: B.R.G.M. Sect. IV, 2, p. 133-152.

Ross, D. J. K., and Bustin, R. M., 2009, Investigating the use of sedimentary geochemical proxies for paleoenvironment interpretation of thermally mature organic-rich strata:

Examples from the Devonian–Mississippian shales, Western Canadian Sedimentary Basin: Chemical Geology, v. 260, p. 1-19.

Rowe, H. D., Hughes, N., and Robinson, K., 2012, The quantification and application of handheld energy-dispersive x-ray fluorescence (ED-XRF) in mudrock chemostratigraphy and geochemistry: Chemical Geology, v. 324-325, p. 122-131.

Sageman. B., and T. Lyons, 2004, Geochemistry of fine-grained sediments and sedimentary rocks. In: Mackenzie, F. (ed.) Sediments, Diagenesis, and Sedimentary Rock: Treatise on Geochemistry, 7. Elsevier, Amsterdam, p. 115–158.

Scholle, P., 1977, Chalk Diagenesis and Its Relation to Petroleum Exploration- Oil from Chalks, a Modern Miracle: AAPG Bulletin, American Association of Petroleum Geologists v. 61, no. 7, p. 982–1009.

Stephenson, L.W., 1952, Larger invertebrate fossils of the Woodbine Formation (Cenomanian) of Texas, USGS Professional Paper 242, 226p and plates.

Tribovillard, N., 2021, Re-assessing copper and nickel enrichments as paleo-productivity proxies: BSGF – Earth Science Bulletin, v. 192.

Tribovillard, N., Thomas, J., Lyons, T., and Armelle, R., 2006, Trace metals as paleo-redox and paleo-productivity proxies- An update: Chemical Geology v. 232, p. 12-32.

Turner, J.R., and S.J. Conger, 1984, Environment of Deposition and Reservoir Properties of the Woodbine Sandstone at Kurten Field, Brazos Co. Texas" The Society of Economic Paleontologists and Mineralogists (SEPM) Siliciclastic Shelf Sediments (SP34), p. 215-249.

Vail, P. R., R. G. Todd, and J. B. Sangree, 1977, Seismic Stratigraphy and Global change of Sea Level, Part 5: Chronostratigraphic Significance of Seismic Reflections: AAPG Memoir, v. 26, p. 99–116, doi: 10.1306/M26490.

Whidden, K.J. et al., 2018, Assessment of Undiscovered Oil and Gas Resources in the Eagle Ford Group and Associated Cenomanian–Turonian Strata, U.S. Gulf Coast, Texas, 2018, USGS Fact Sheet 2018–3033, 4p., at https://doi.org/10.3133/fs20183033.

Zhang, X., 2017, High Resolution Stratigraphy and Facies Architecture of Buda Formation in Central Texas. [master's thesis]: Texas A&M University, College Station, Texas, 59 p.

Zuckerman, G., 2014, The Frackers, Penguin Group, New York, 747p.

APPENDIX A FIGURES

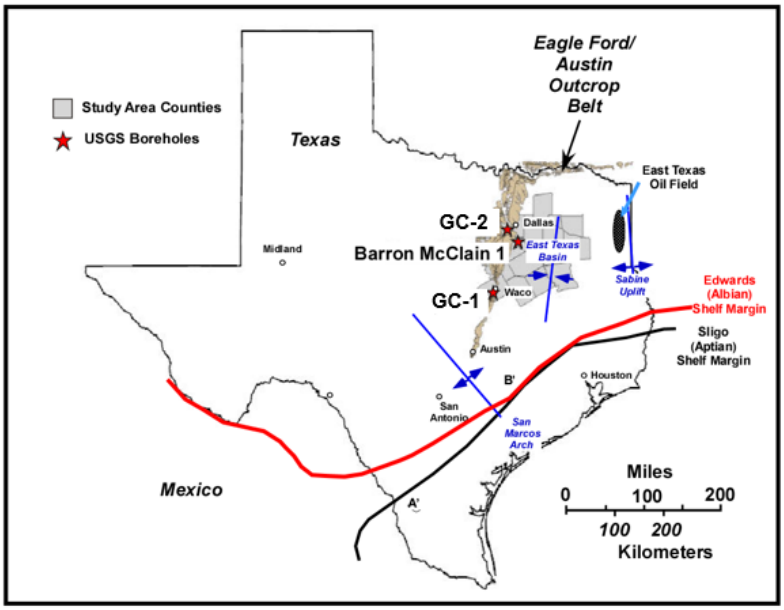

Figure 1: Study area map with borehole locations (stars), the Eagle Ford Group/Woodbine Group outcrop belt (light brown) and important structural features that bound the East Texas Basin (ETB). Counties in the study area are gray polygons. The ETB is bounded to the North and West by the Middle Cenomanian Outcrop Belt, to the east by the Sabine uplift, to the southeast by the Edwards and Sligo Shelf Margins, and to the southwest by the San Marcos Arch.

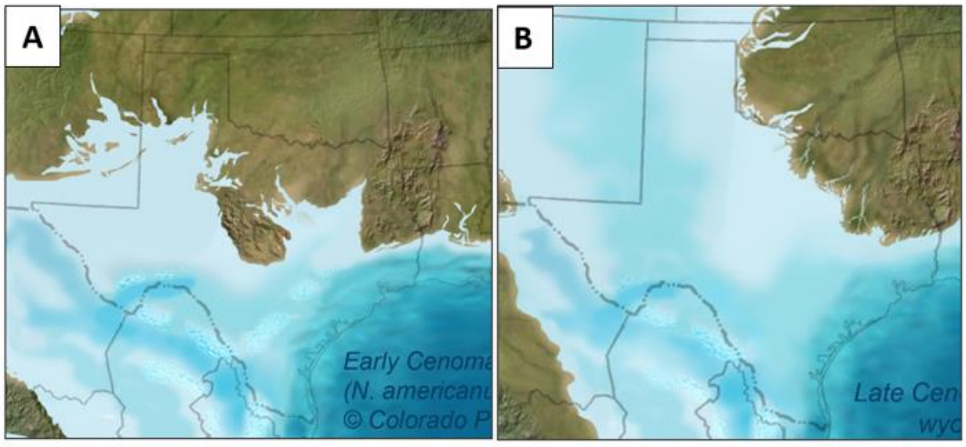

Figure 2: Blakey Paleogeography maps of Texas in the Early Cenomanian at ~98.1 Ma, the beginning of Woodbine deposition (A) and ~94.9 Ma, Early Turonian, during Eagle Ford Deposition. (Blakey, 2019)

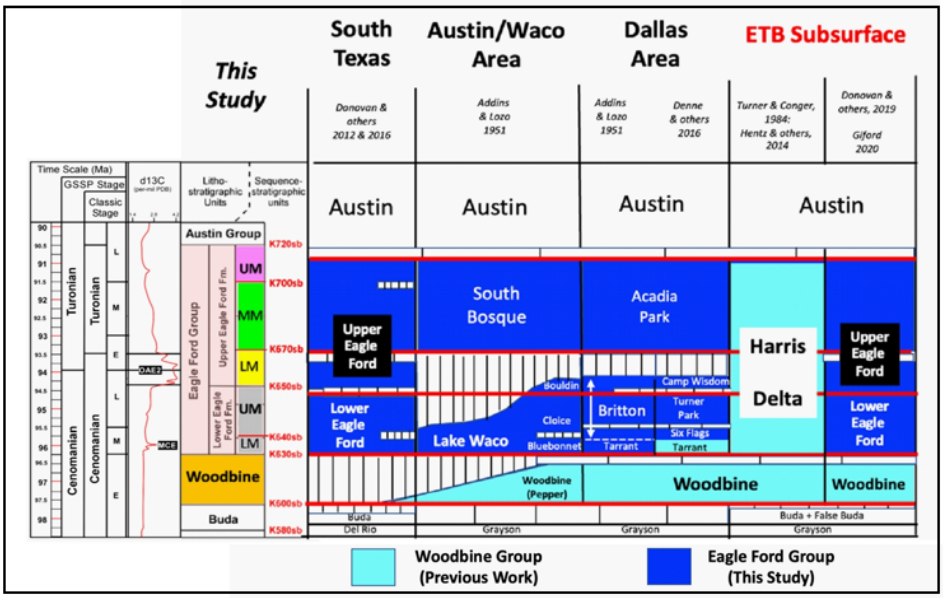

Figure 3: Generalized stratigraphic column showing Classic and New ICS stages, δ13C global isotope profile (Ogg and Hinnov, 2012) alongside nomenclature from studies across the ETB. Colored boxes in this study's nomenclature represents the colors of the units in the presented cross sections (Figures 10 and 11). This chart is a summary of the differences in stratigraphic assignment of the same Cenomanian-Turonian units across studies across Texas and over time. The dark blue was assigned to the Eagle Ford Group and light blue to the Woodbine Group. The most unique interpretation is the assignment of the Harris Delta to the Woodbine group, which is interpreted to be in the upper formation of the Eagle Ford Group in this study.

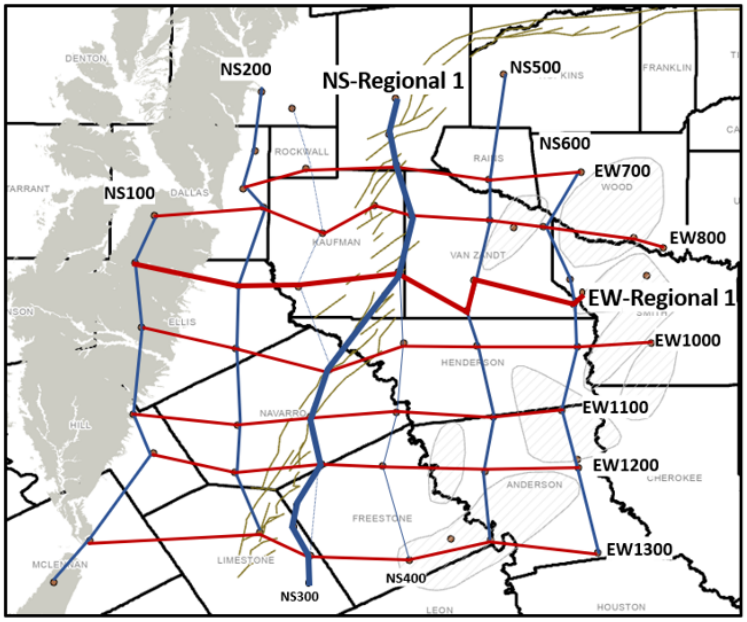

Figure 4: Grid of cross sections across the study area with the Middle Cretaceous outcrop belt (light gray polygon), the Mexia-Talco fault zone (brown lines), and the Luann salt domes (light gray hatched shapes). North-south lines are in dark blue. West – east lines are in red. Type Sections NS-Regional 1 and EW-Regional 1 are bolded lines

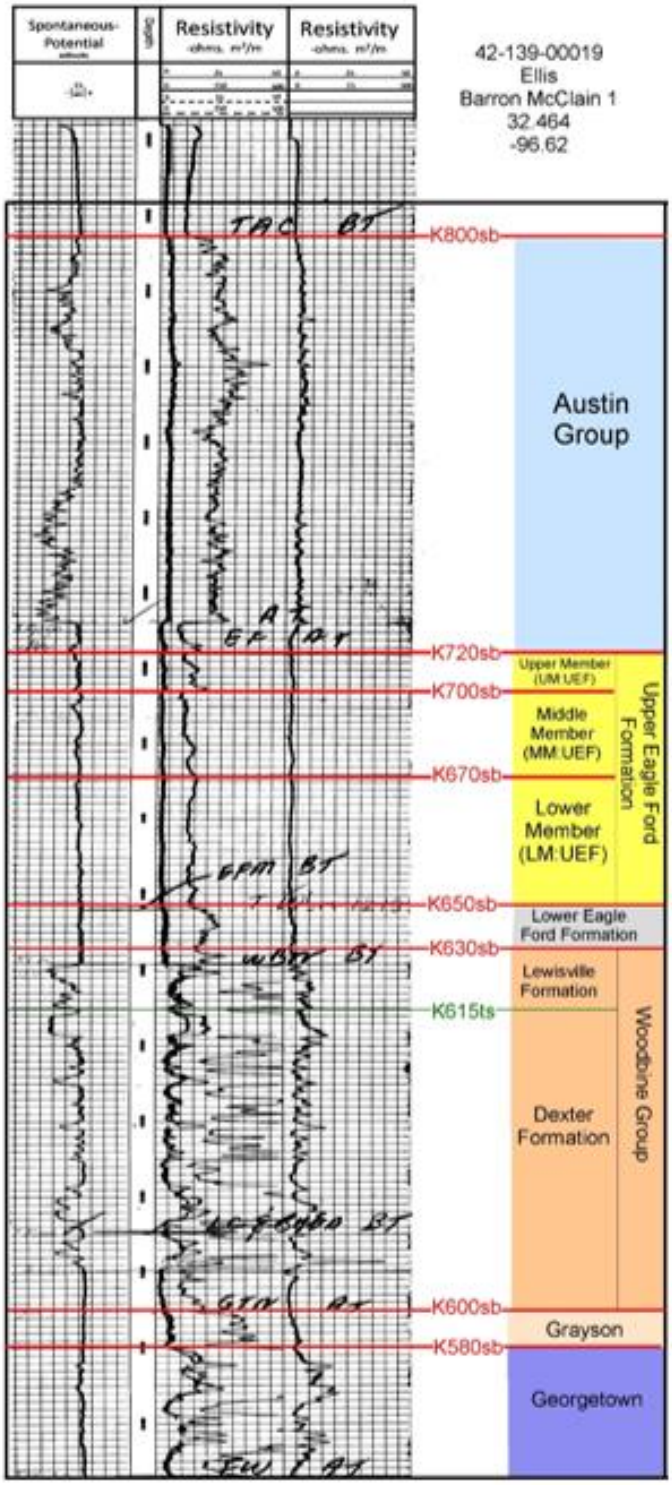

Figure 5: Stratigraphic column of units in this study alongside the Barron McClain 1 well logs . Cuttings were taken every 10'. This type log represents the typical SP and resistivity response for the various the formations and members.

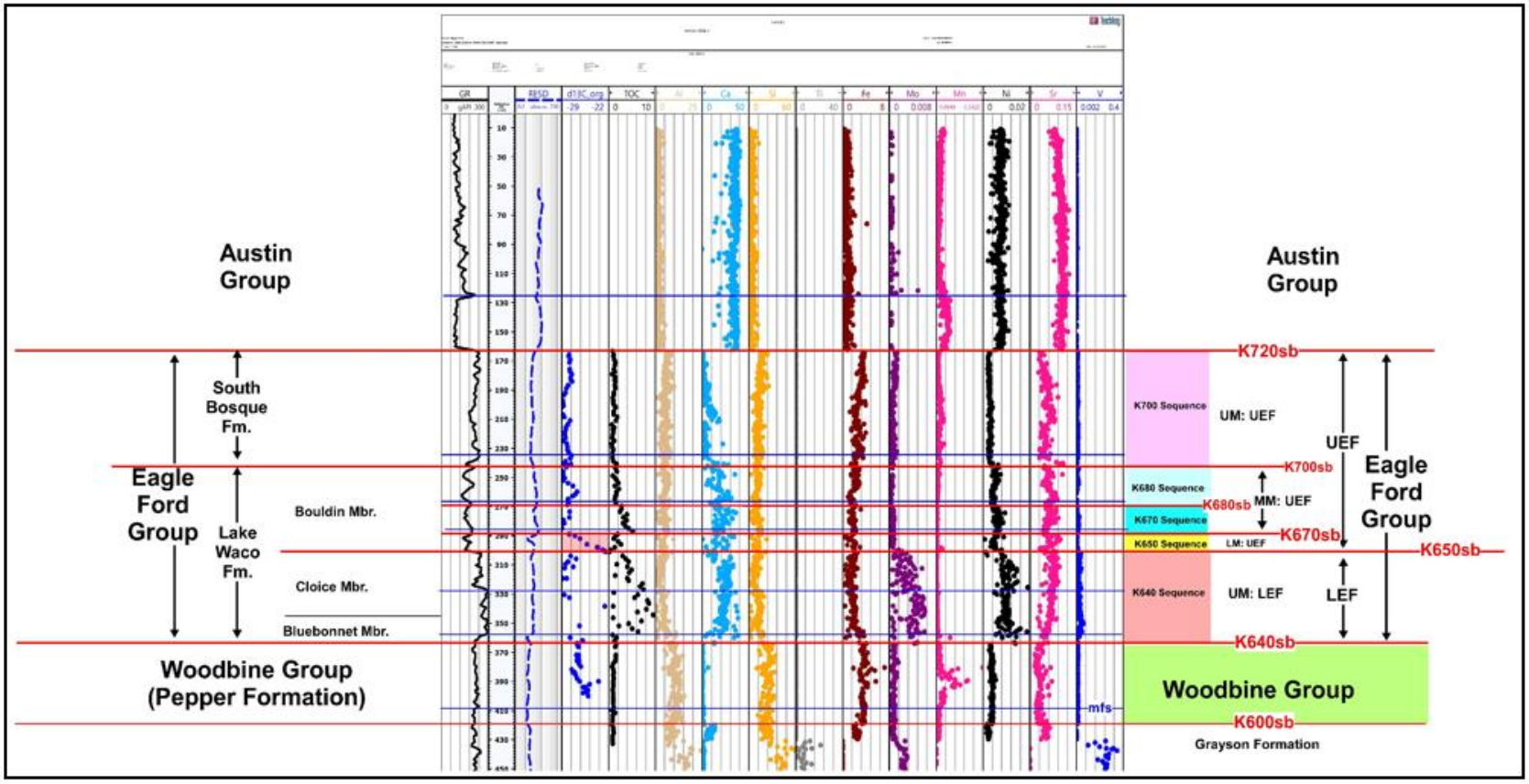

Figure 6: XRF element concentrations for the GC-1 core, taken near Waco, with stratigraphic nomenclature from past studies on the left and this studies sequence stratigraphic framework on the right. Note that the LM: LEF does not occur in this well. The Woodbine Group is best described as Ca, Mo, Ni, and V – poor with high Si. The organic-rich LEF has high Ca, Mo, and Ni. The UEF is TOC-poor and decreases in Ca content toward the top. The LM:UEF is only 12' thick, but the positive $\delta^{13}C$ isotope excursion can be seen.

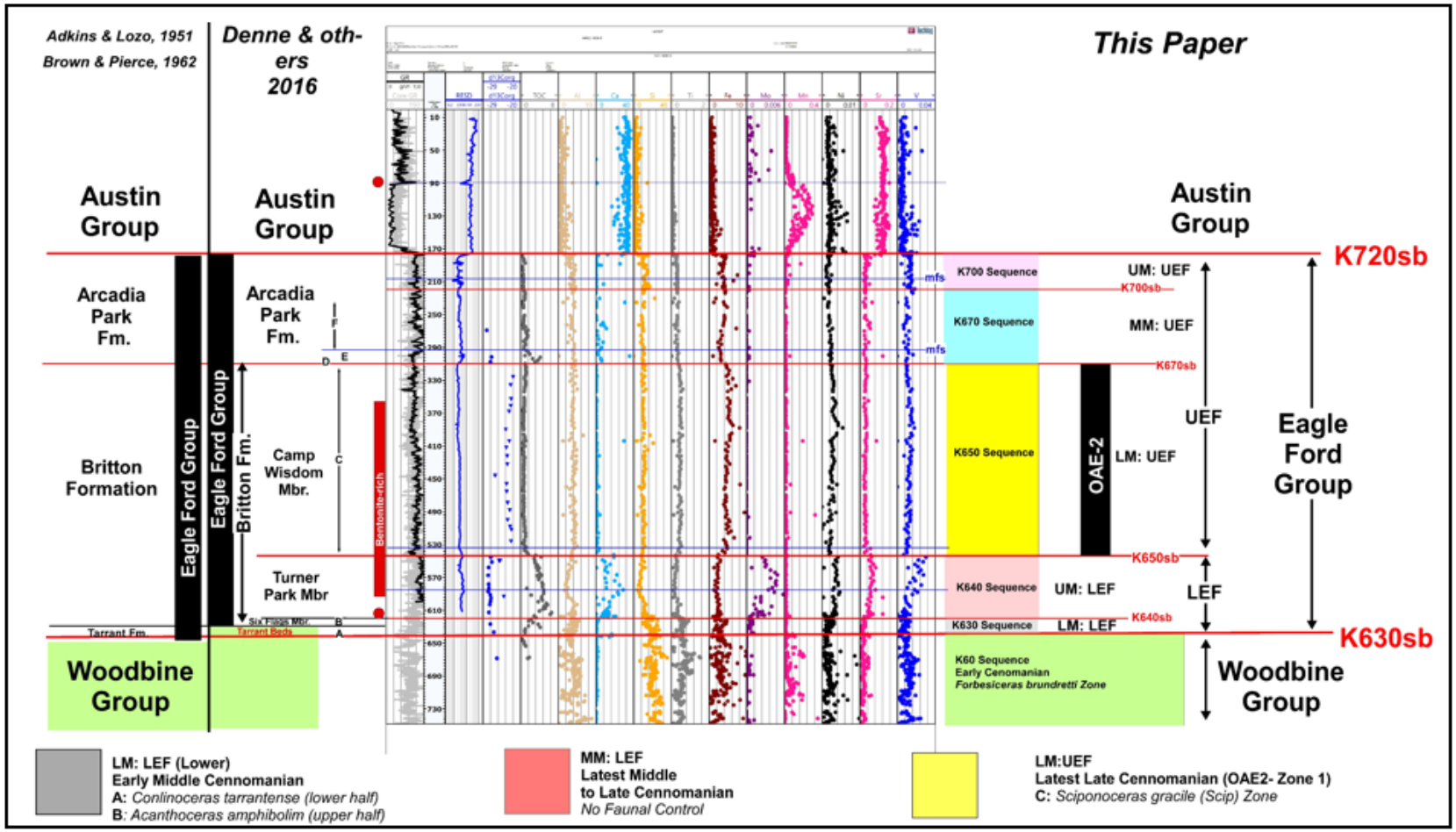

Figure 7: XRF element concentrations for the GC-2 core, drilled near Dallas, with stratigraphic nomenclature from past studies on the left and this studies stratigraphic framework on the right. This well experienced borehole problem during logging, but core gamma ray supplemented the UM:LEF to upper Woodbine interval. The Woodbine Group is best described as Ca, Mo, Ni, and V poor with high Si. The LM:LEF is equivalent to the Tarrant Beds and is Ca poor with some TOC. The UM:LEF is Ca and TOC rich. The LM:UEF shows the positive $\delta^{13}C$ isotope excursion. Some ammonite markers (Kennedy, 1988) also are displayed, including *Conlinoceras tarrantense,* which appears in both the Gulf Coast and KWIS regions, signaling the time when the KWIS extended from the Arctic to the Gulf of Mexico.

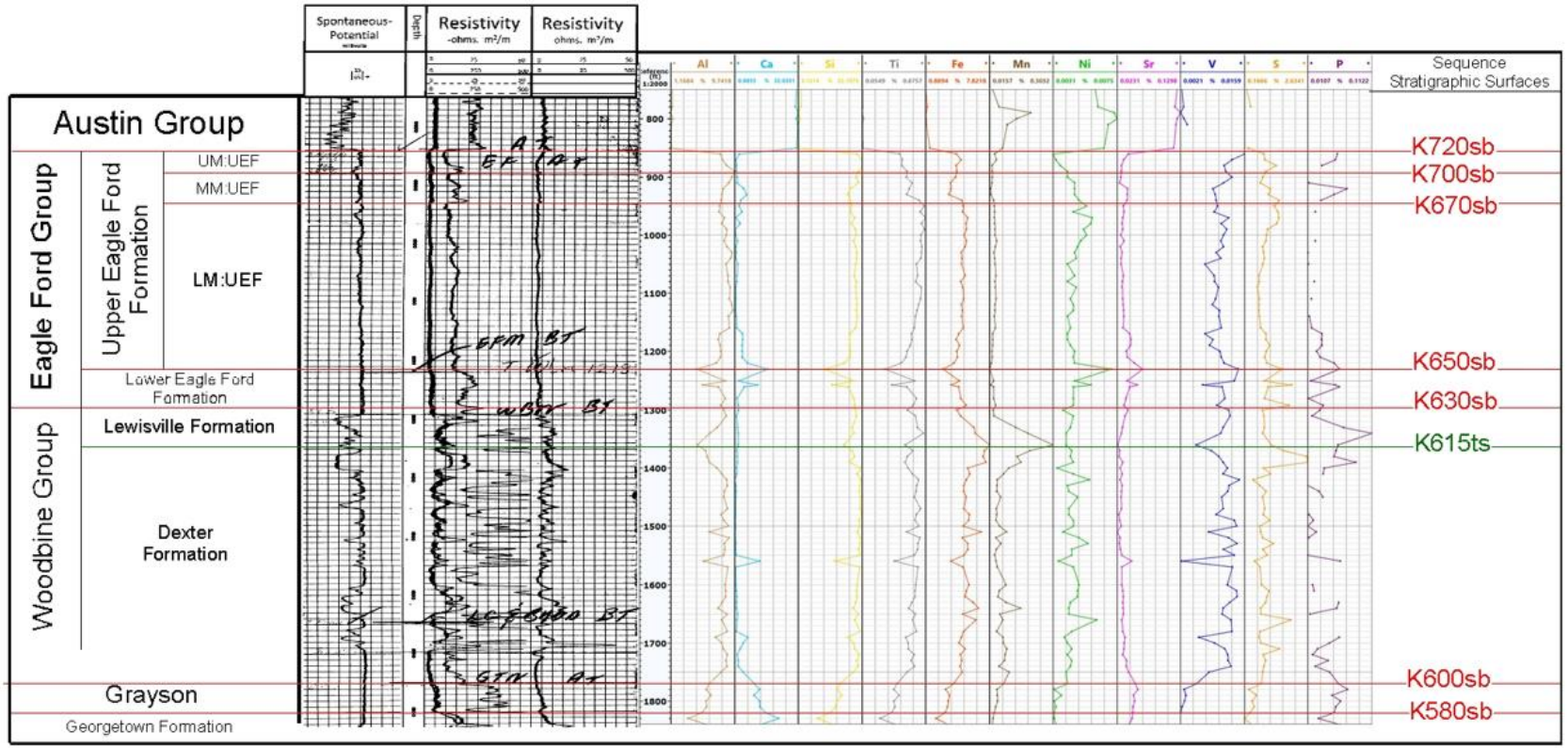

Figure 8: XRF element concentrations for the Barron McClain 1 well cuttings, taken from Ellis County, with this study's stratigraphic framework on the right. Cuttings were taken every 10' and made into pellets to be scanned. These cuttings allowed for detailed comparison of the Woodbine formations. The Dexter and Lewisville are not geochemically different, but the K615ts boundary between them is uniquely characterized by a drop in Al and V, and a rise in Fe, and Mn. The LEF is Ca, Mo, and V rich when compared to the UEF.

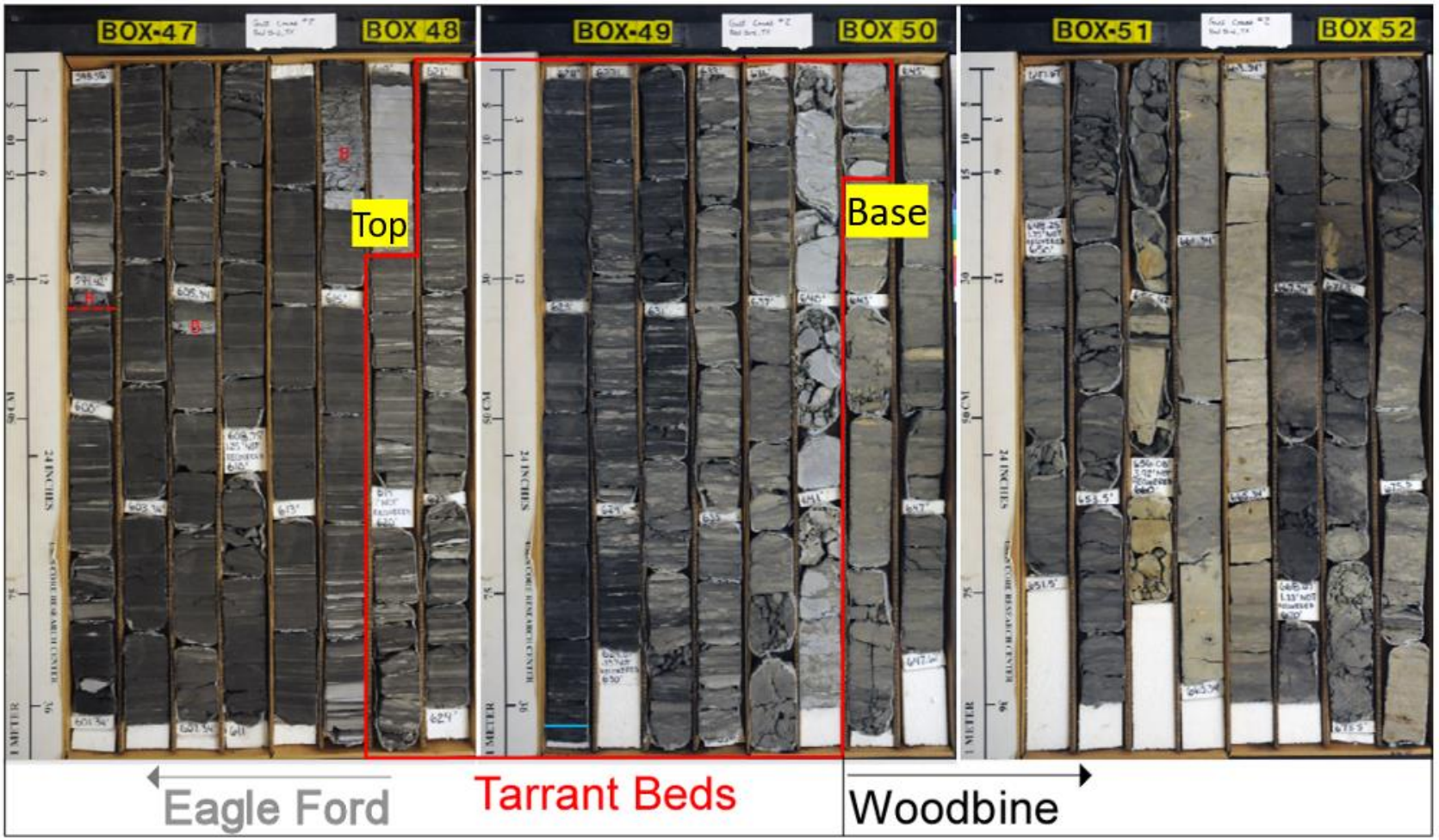

Figure 9: Core photos from GCA-2 that show the Tarrant Beds with the overlying remainder of the Eagle Ford Group on the left and the underlying Woodbine group on the right. Seen here is the transition from fossiliferous marine strata of Eagle Ford Group (right) to un-fossiliferous mudstones and sandstones of the (left). The base is marked by a distinct cobble bed that overlies the K630sb.

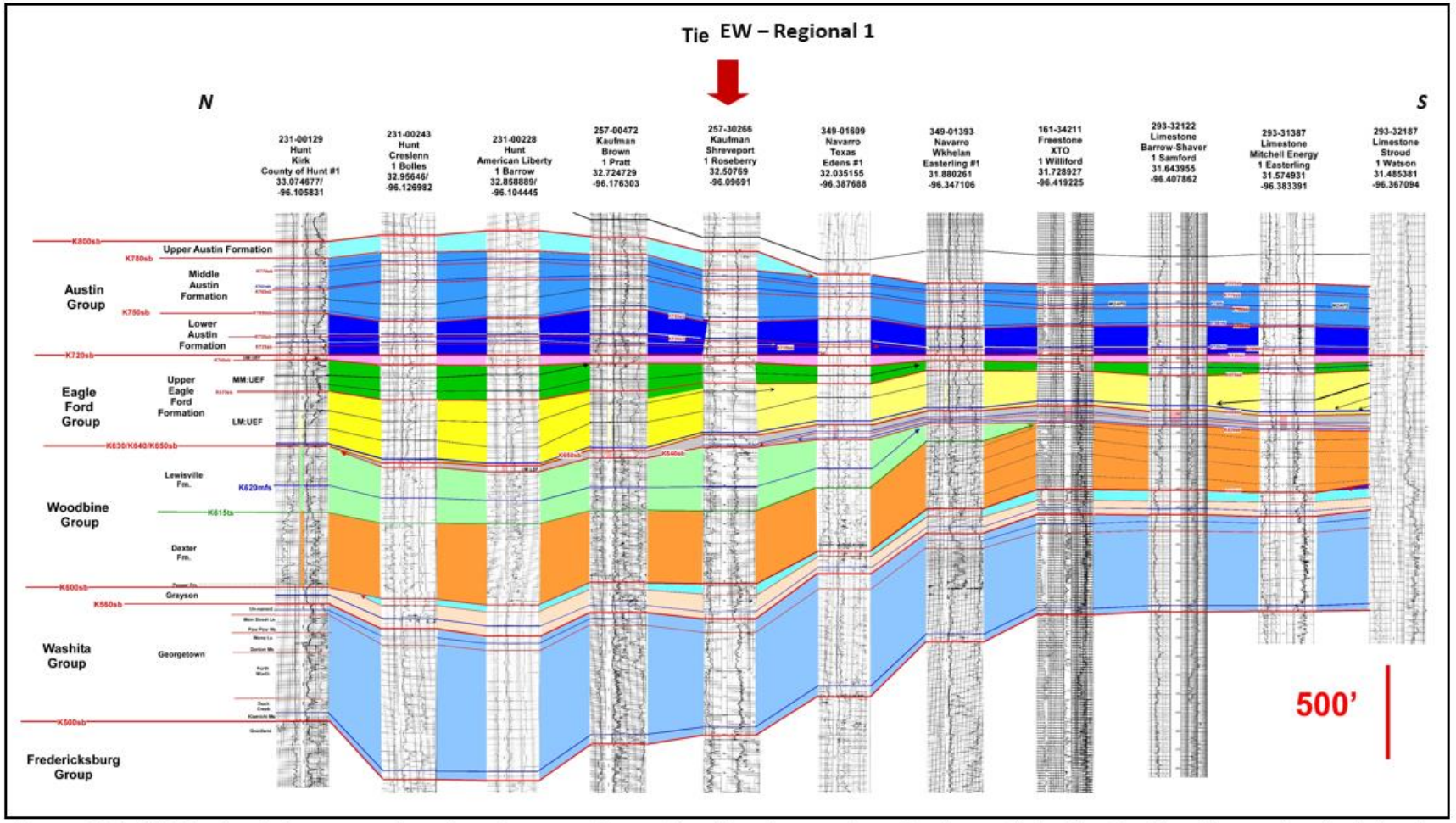

Figure 10A: NS-Regional 1; type regional north to south trending line datumed on the base of the Austin. Notable results include the southern truncation of the Buda by the K600sb, the southern truncation (thinning) of the Woodbine (Lewisville) beneath the K630sb, and the northerly truncation (thinning) of the LEF beneath the K650sb at the base of the UEF. Angular disconcordance is shown under the K630sb.

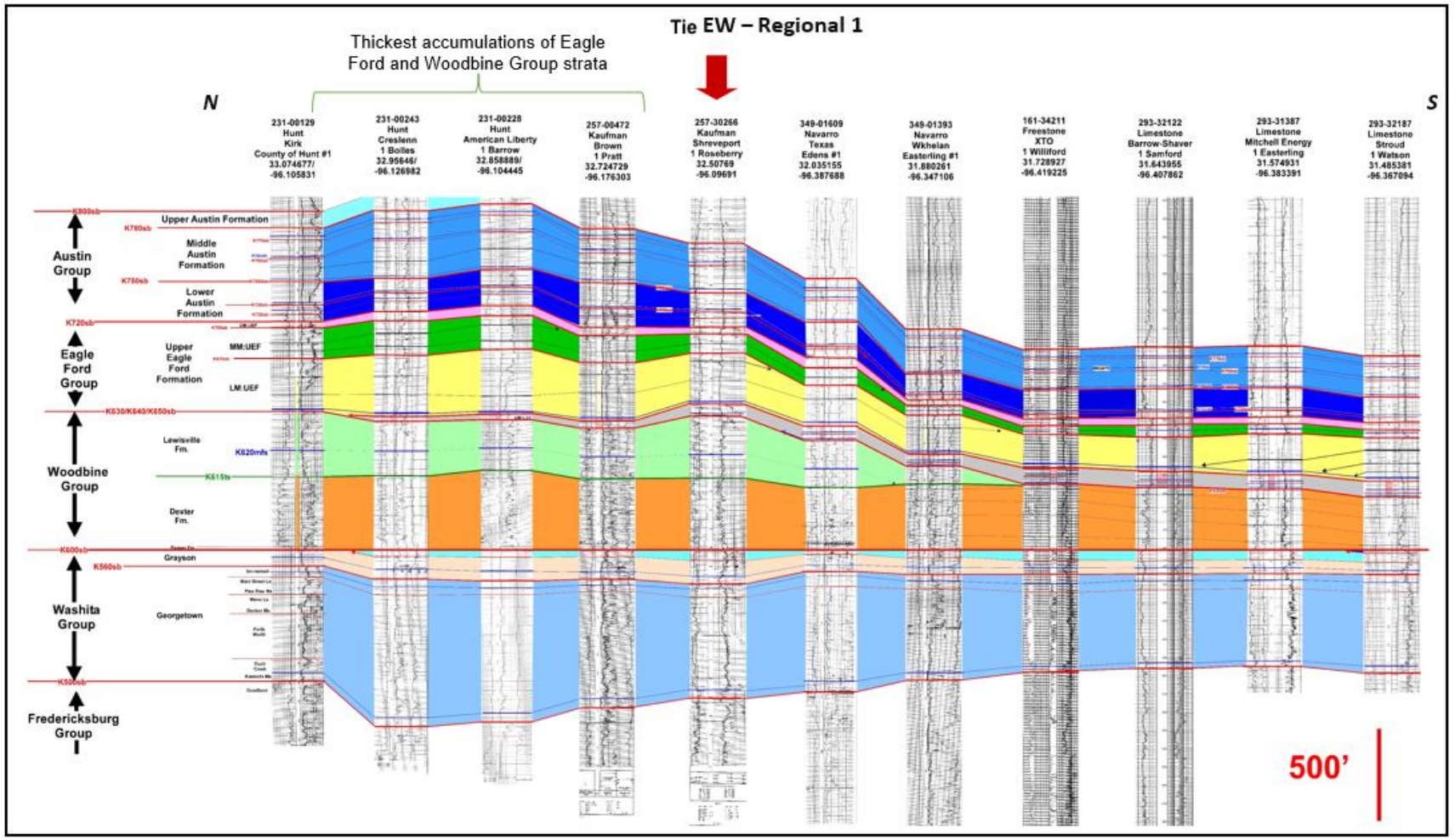

Figure 10B: NS-Regional 1; type regional north to south trending line datumed on the base of the Woodbine. This cross section highlights that the thickest accumulations of both Eagle Ford Group and Woodbine Group strata occur to the north towards Hunt county (marked by green bracket).

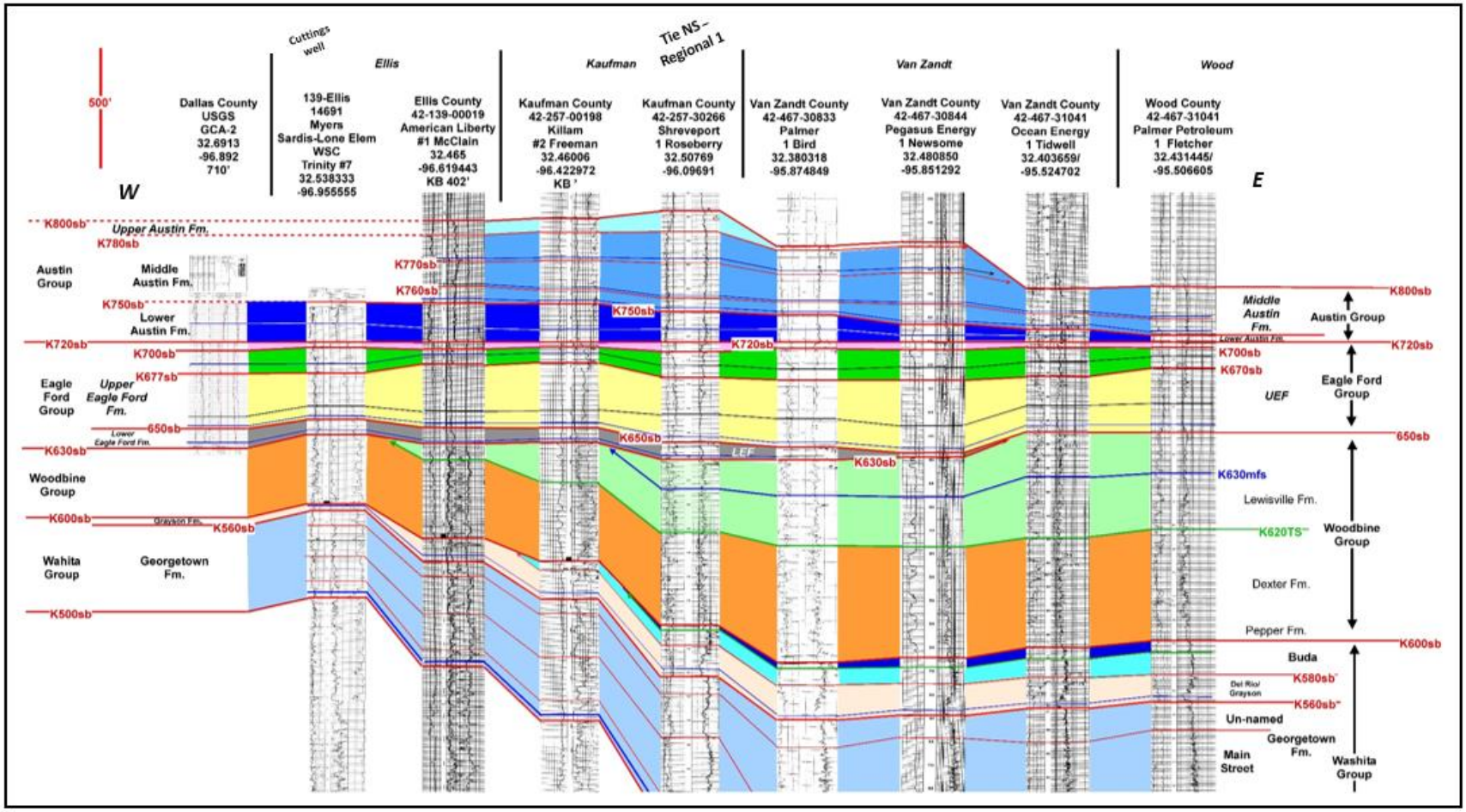

Figure 11A: EW-Regional 1; type regional east to west trending line datumed on the base of the Austin. Notable results include the western truncation of the Buda beneath the K600sb, the western truncation (thinning) of the Woodbine (Lewisville) beneath the K630sb, and the eastern truncation (thinning) of the LEF beneath the K650sb at the base of the UEF. Angular disconcordance is shown under the K630sb.

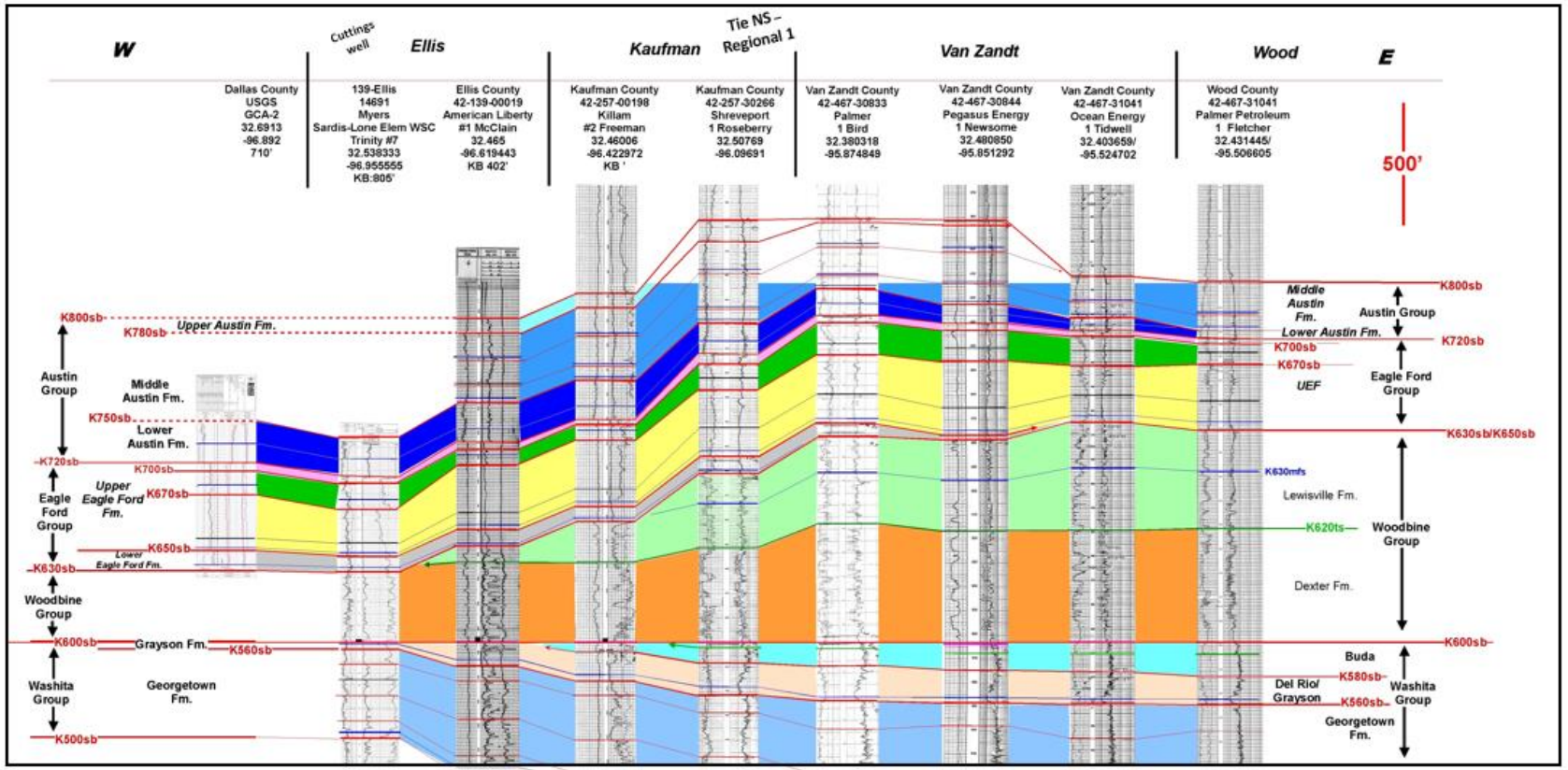

Figure 11B: EW-Regional 1; type regional east to west trending line datumed on the base of the Woodbine. This cross section highlights that the thickest accumulations of both Eagle Ford and Woodbine strata occur with Van Zandt county.

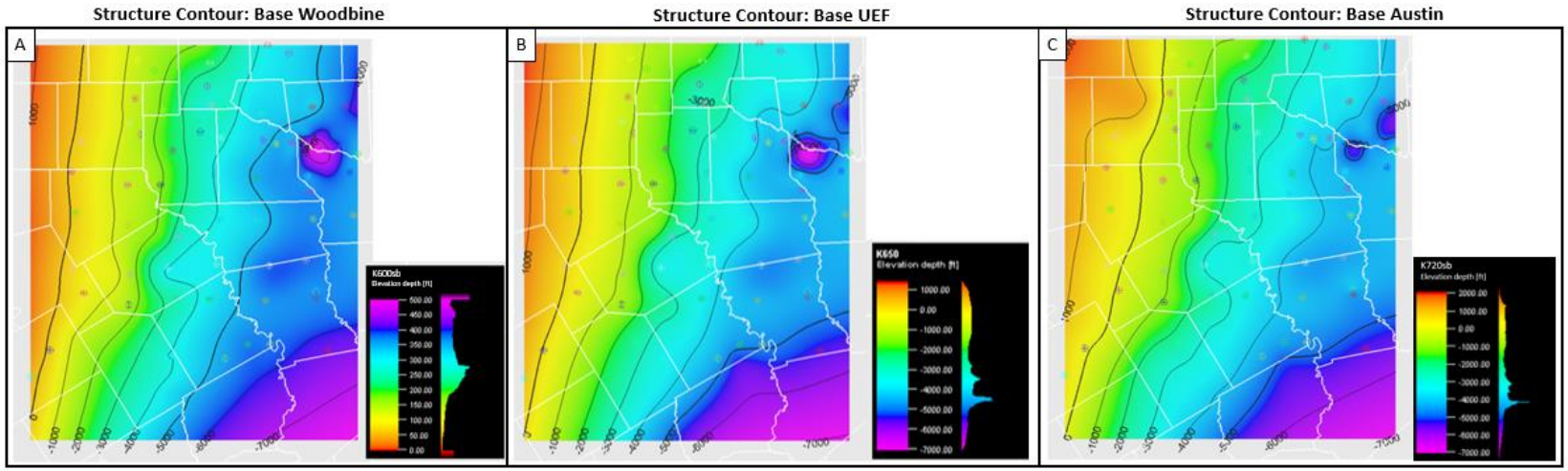

Figure 12: Structure contour maps for the (A) the K600sb/base of the Woodbine Group, (B) K650sb/base of the UEF and, (C) K720sb/base of the Austin. Contours are in feet (SSTVD) and well location are noted by small colored circles. Contour interval is 1,000' All illustrate a similar trend. The basin dips to the east, as well as to the south, with the deepest portions of the basin in the southwest portions of the study area

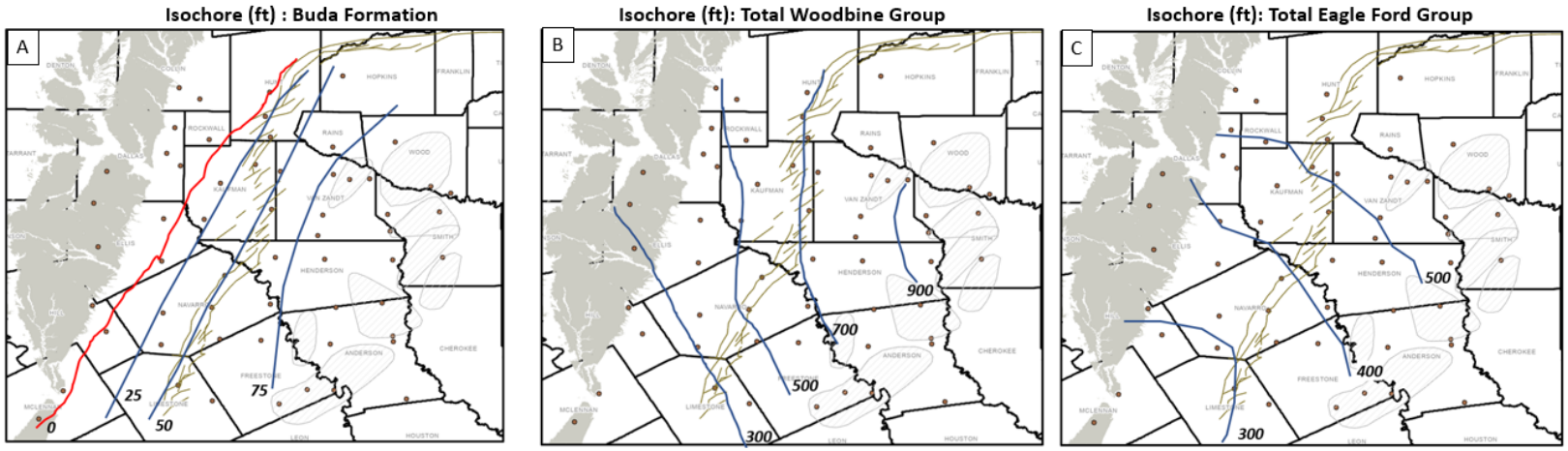

Figure 13: Isochore map of the (A) Buda Formation, (B) Woodbine Group, and (C) Eagle Ford Group. Contours are in feet and well location are noted by the small brown circles. Contour intervals are 25' (Buda), 200' (Woodbine), and 100' (Eagle Ford). The structurally updip limit of the Buda is lined in red. The Woodbine and Buda thicken to the east and the Eagle Ford thickens to the northeast.

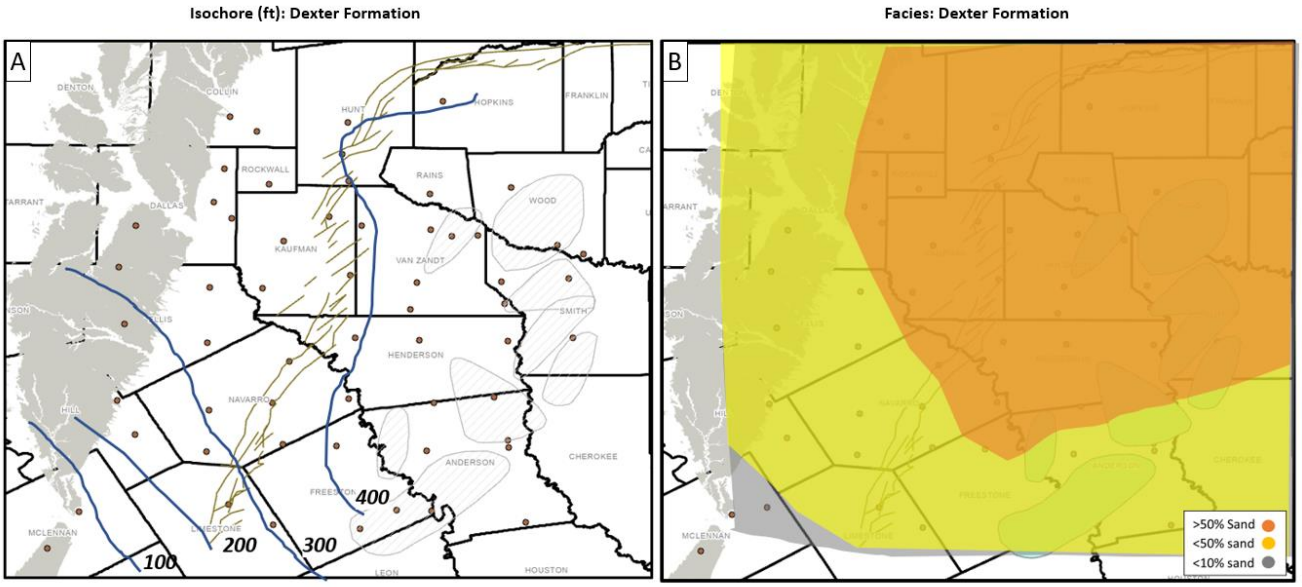

Figure 14: Isochore (A) and facies map (B) of the Dexter. Contours are in feet and well location are noted by the small brown circles. Contour interval is 100'. The gray color is less than 10% sand, the yellow is between 10%-50% sand, and the orange is >50% sand. The Dexter is thickest to the east and thins to the southwest. The northeast section is most sand-dominated.

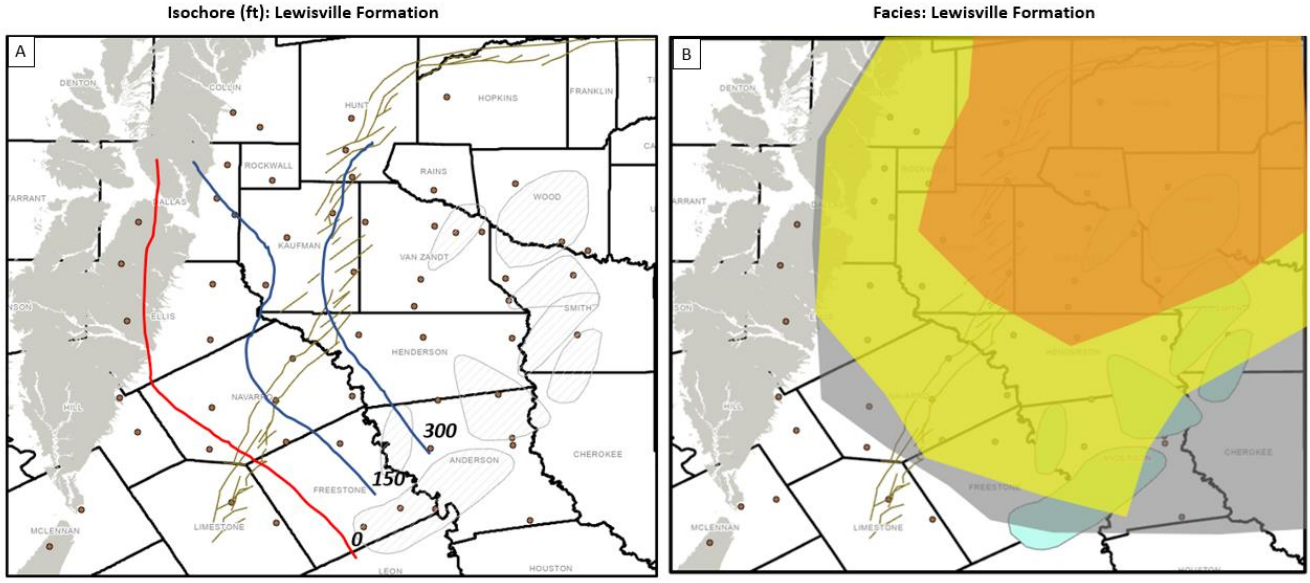

Figure 15: Isochore (A) and facies map (B) of the Lewisville. Contours are in feet and well location are noted by the small brown circles. The truncation of the Lewisville Formation is lined in red. The contour interval is 150'. The Lewisville is thickest and sand-dominated to the northeast. On the facies map, the gray color is less than 10% sand, the yellow is between 10%-50% sand, and the orange is >50% sand.

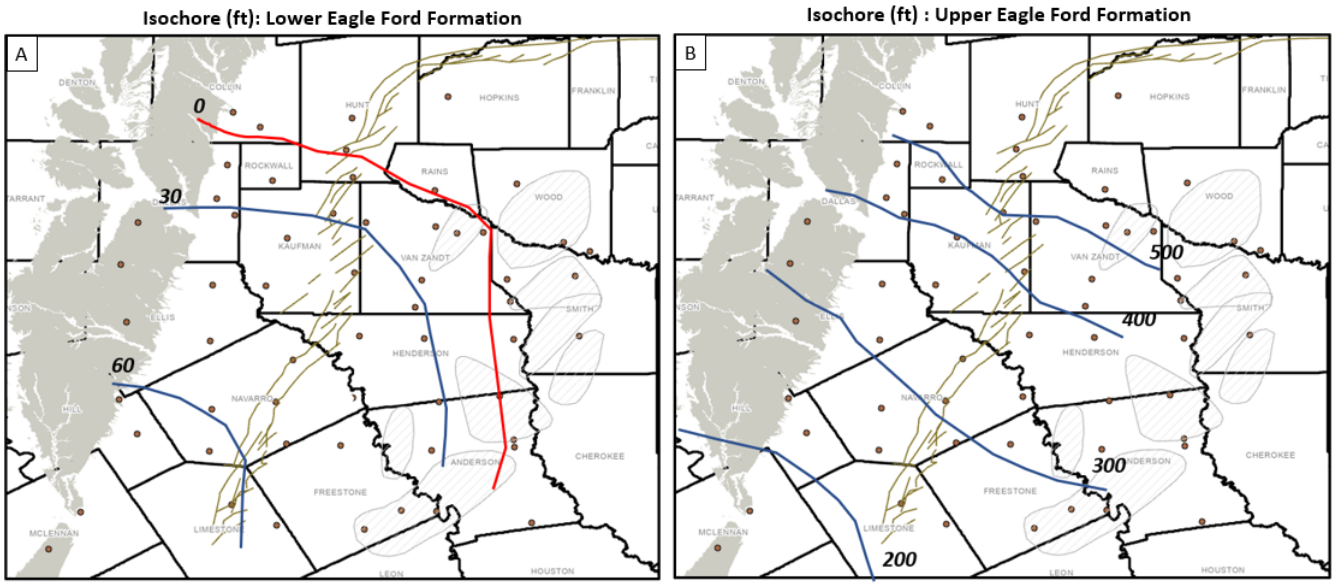

Figure 16: Isochore maps of the (A) LEF and the (B) UEF. Contours are in feet and well location are noted by the small brown circles. The contour interval for the LEF is 30' and the UEF is 100'. The truncation of the LEF is lined in red to the north and west. The LEF is thickest to the southwest, while the UEF is thickest to the northeast.

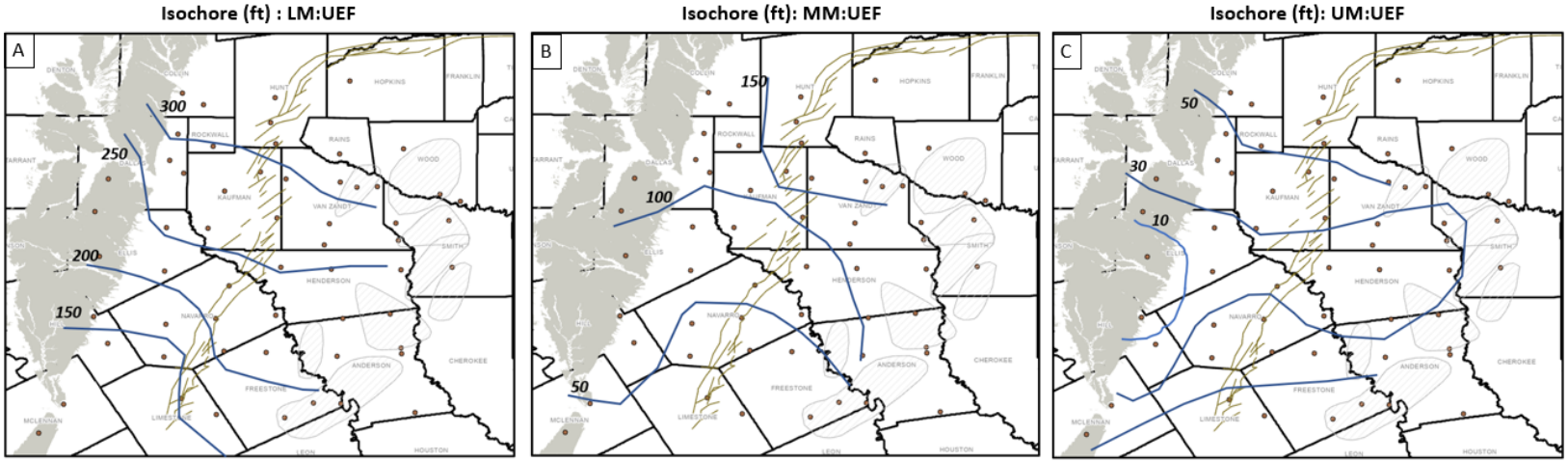

Figure 17: Isochore maps of the three UEF members: LM:UEF (A), MM:UEF (B), and UM:UEF (C). Contours are in feet and well location are noted by the small brown circles. Contour intervals are 150' (LM:UEF), 50' (MM:UEF), and 20' (UM:UEF). Generally, all three members thicken to the northeast. The LM:UEF is the thickest overall and contains sands that are coeval to the Harris Delta.

Facies Map: LM:UEF and Harris Delta (Gifford, 2021)

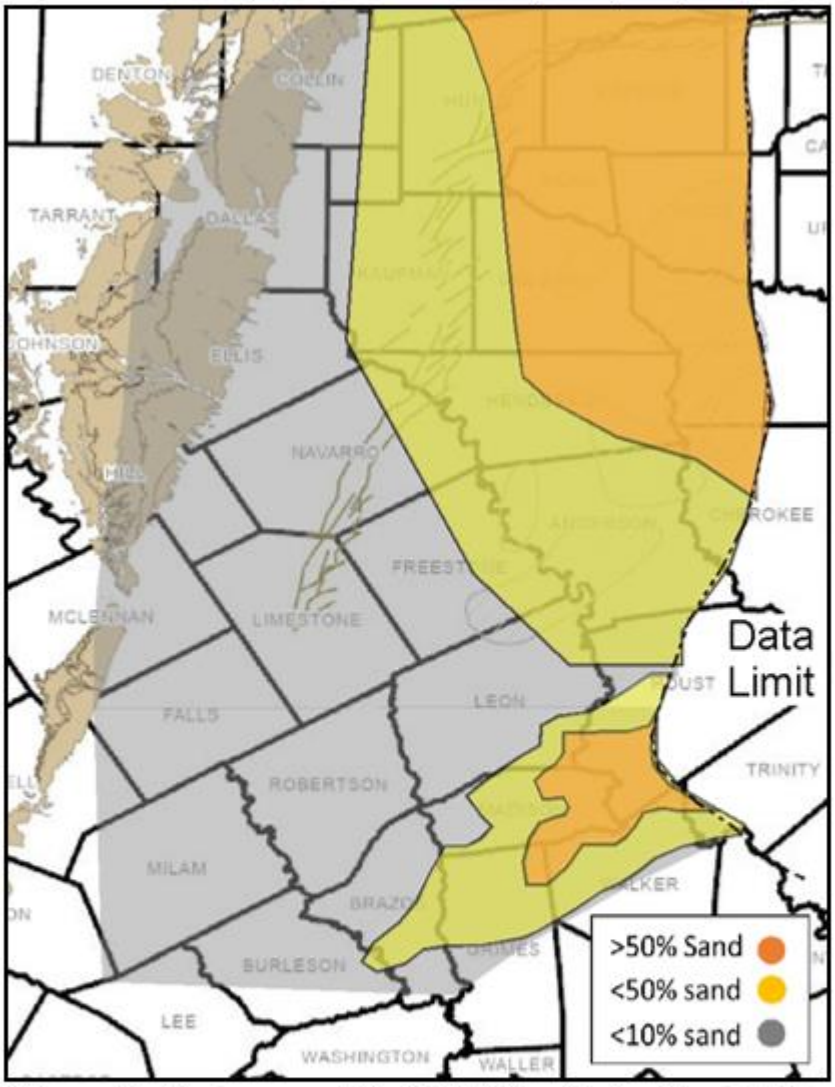

Figure 18: Facies map of the LM:UEF with the Harris Delta as mapped in Gifford (2021). The gray color is less than 10% sand, the yellow is between 10%-50% sand, and the orange is >50% sand. With the LM:UEF being coeval to the Harris Delta, this work extends the sand play of this sequence to the northeast.

Element	Mineralogy	Proxy	Interpretation	References
Al Aluminum	Clay minerals. Illite Group. Glauconite.	Clay and Feldspar	Concentration of clay and feldspars in limestones can be used to help identify sections of clay input and interbedded marls.	Pearce & Jarvis (1992); Tribovillard *et al.* (2006)
Ca Calcium	Calcite ($CaCO_3$), Calcium orthophosphates ($CaPO_4$)	Carbonate source and Phosphate accumulation	Calcium is primarily a proxy for calcite and calcareous input in limestones.	Banner (1995); Tribovillard *et al.* (2006)
Si Silicon	Quartz (SiO_2)	Quartz	Silica is used as a proxy for quartz and terrigenous input.	Pearce & Jarvis (1992); Sageman & Lyons (2004)
Ti Titanium	Detrital sediments (Ti^{4+}, Rutile (TiO_2), and Ti-bearing minerals)	Continental source and dust fraction; Intensity of chemical weathering	Titanium and other detrital elements are used as proxies to interpret depositional processes, like source origin and weathering, versus paleooceanographic conditions	Calvert & Pedersen (1993); Sageman & Lyons (2004); Ross & Bustin (2009)
Ni Nickel	$NiCO_3$, Ni^{2+}, $NiCl^{+}$ (oxic conditions); NiS (sulfate reducing conditions)	Organic matter/micronutrient availability in the water column	Ni is soluble in oxygenated water columns and behaves as a micronutrient for microbial scavengers. In stratified water columns or upwelling, scavengers will ingest Ni in oxygenated surface waters and will be deposited and preserved at the anoxic sediment-water interface. Enriched in sediments rich in organic matter.	Tribovillard *et al.* (2006) Tribovillard (2021)
Fe Iron	Pyrite (FeS2), Ferroan Dolomite ($Ca(Mg,Fe)(CO_3)_2$), Siderite ($FeCO_3$)	Redox sensitive	Trace metals that are redox sensitive are useful for characterizing oxic/suboxic/anoxic paleooceanographic conditions during time of deposition. Iron reduction releases high concentrations of Fe2+. Pyrite can form in most environments	Tribovillard *et al.* (2006) Canfield and Raiswell (1998)
S Sulfur	Pyrite (FeS_2)	Redox sensitive	Trace metals that are redox sensitive are useful for characterizing oxic/suboxic/anoxic paleooceanographic conditions during time of deposition.	Tribovillard *et al.* (2006) Canfield and Raiswell (1998)
Mn Manganese	MnO_2, Mn^{2+}/Mn(IV), and Mn(II) oxides	Redox sensitive, Mn-enrichment during oxic bottom water conditions.	The mobile nature of Manganese in reducing conditions allows for ease of transfer of trace metals out of the water column and into the depositing sediment. Upwelling sediments are low in Mn-enrichment.	Calvert & Pedersen (1993); Sageman & Lyons (2004); Brumsack (2006)
Sr Strontium	Sr-Ca substitutes in calcite, aragonite and dolomite	Carbonate source and phosphate. Affinity towards calcium carbonate	With an affinity for substitution in carbonate forming minerals, Strontium is used as a proxy for carbonate source and diagenetic influence.	Scholle (1977); Renard (1979); Banner (1995);
V Vanadium	HVO2-4 and H2VO-4 (oxic) VO2-, VO(OH)-3, VO(OH)2 (mildly reducing)	Bottom water anoxia, redox sensitive. Authigenic organometallic input	Redox sensitive trace metals help determine paleoceanographic conditions during deposition. Enrichment of Vanadium occurs in suboxic-anoxic conditions because it is immobile in low oxygen, restricted environments.	Sageman & Lyons (2004); Algeo and Rowe, 2012

Table 1: XRF geochemical proxy interpretation table and references (Modified from McCreary, 2022)

APPENDIX C SUPPLEMENTARY MATERIAL

Pellets made from the Barron McClain 1 well cuttings

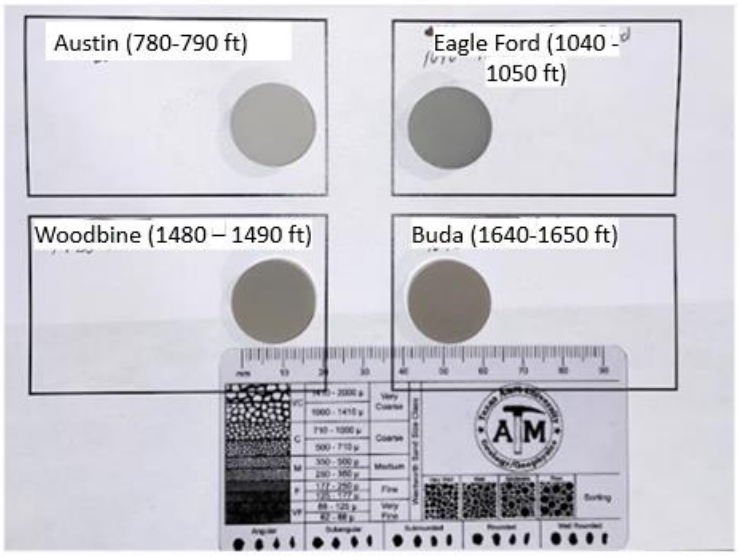

APPENDIX

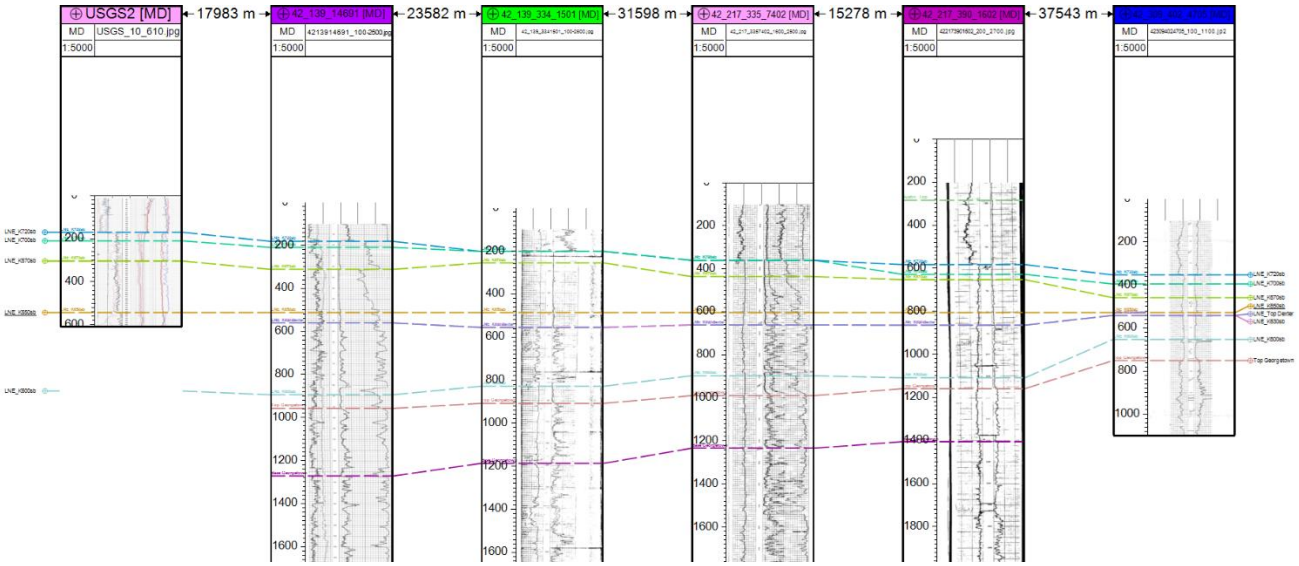

Above: NS100

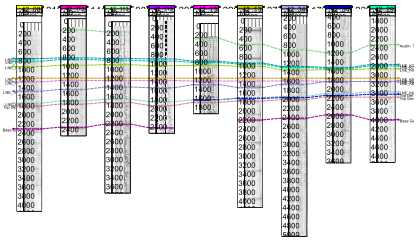

Above: NS200

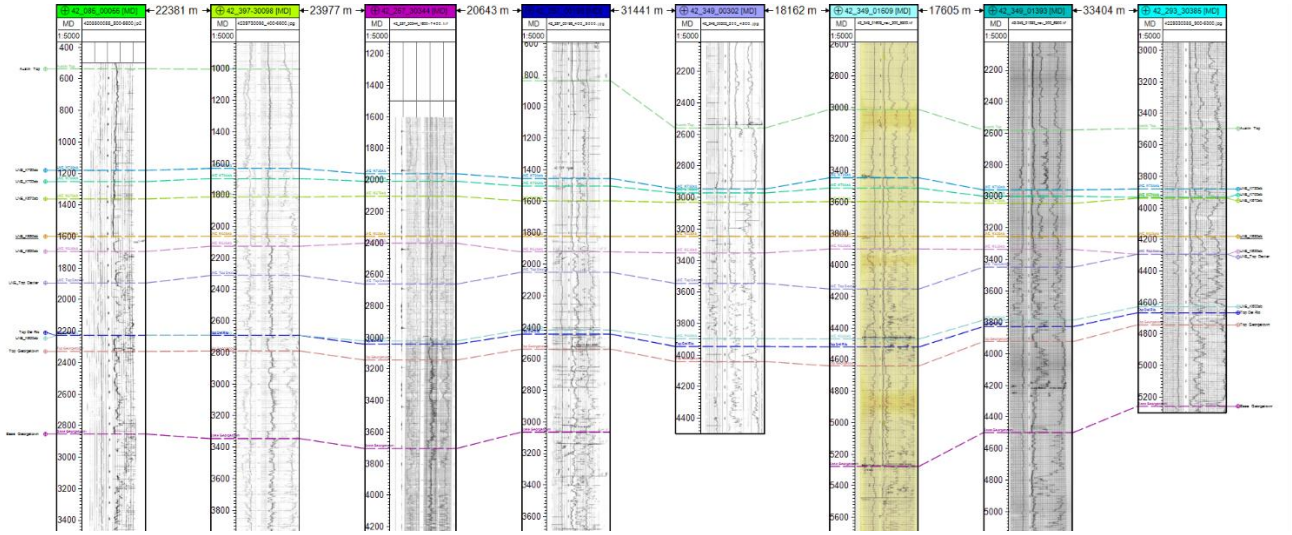

Above: NS300

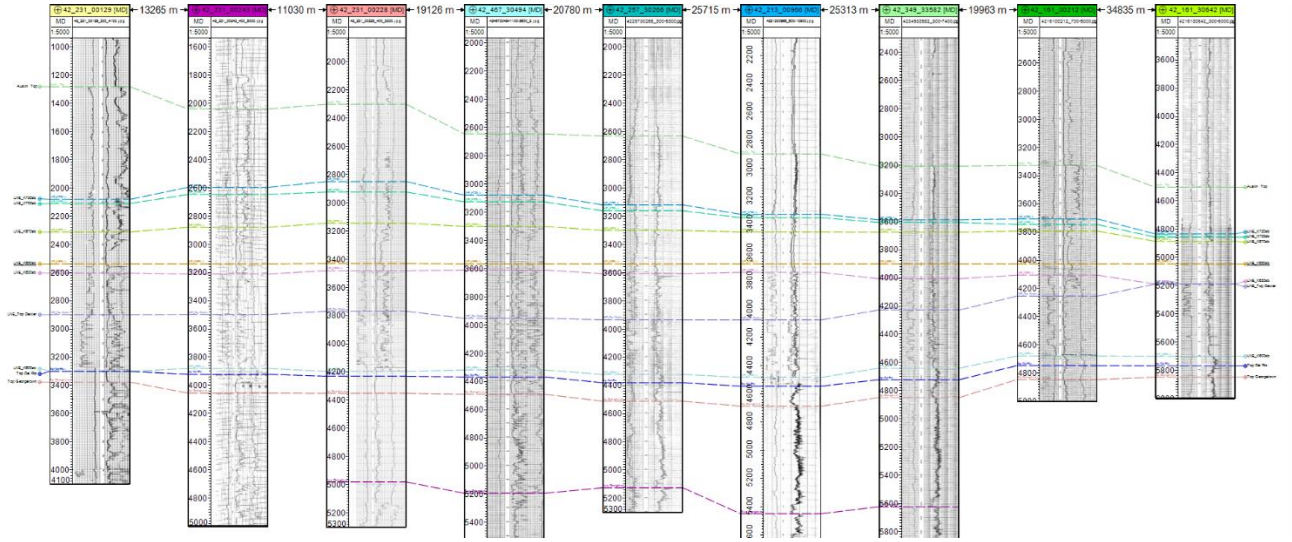

Above: NS400-2

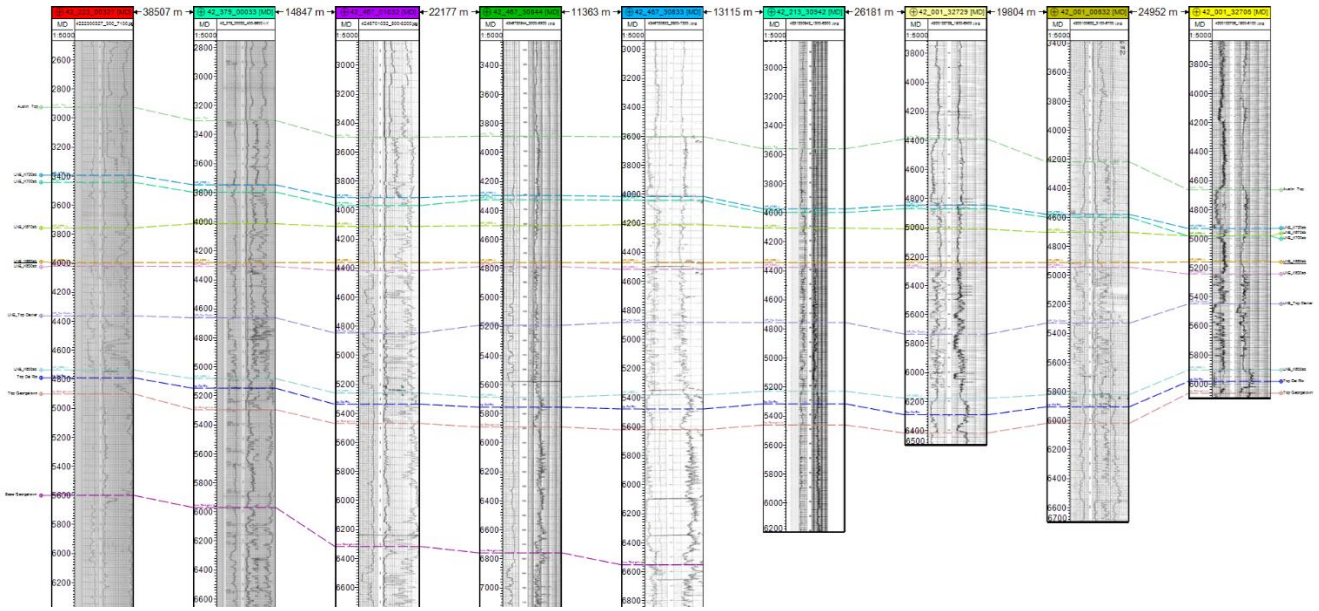

Above: NS500

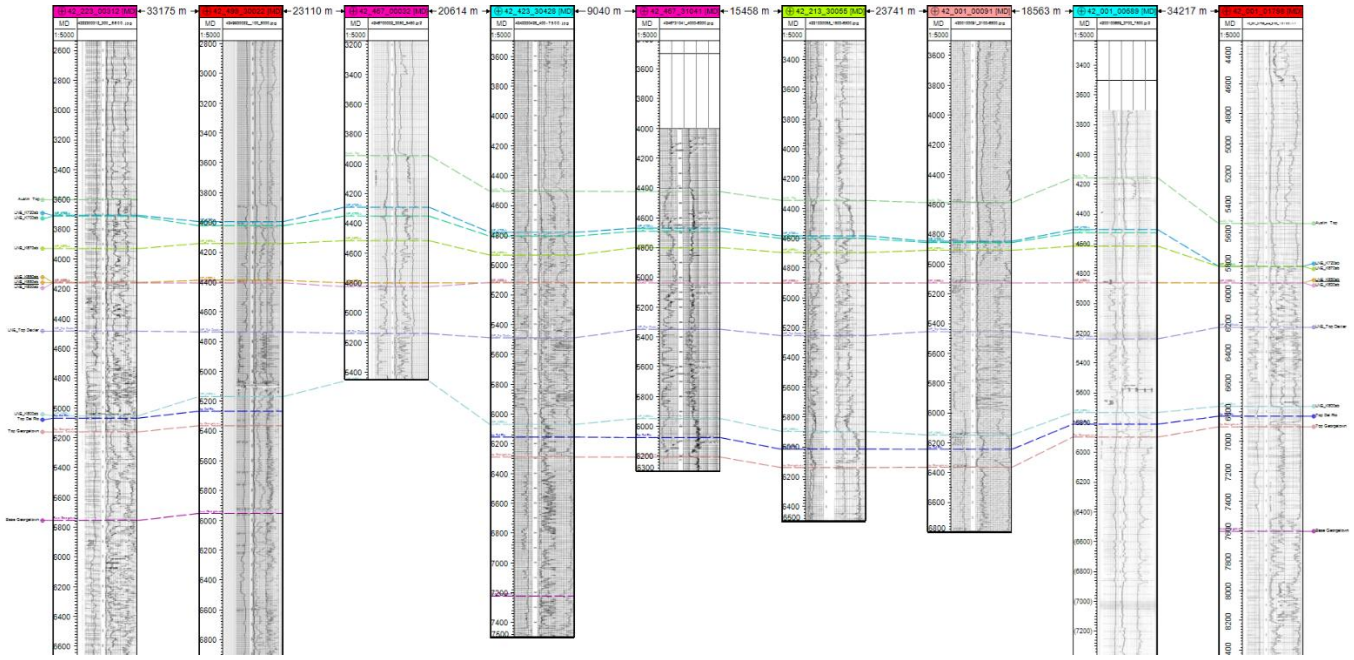

Above: NS600

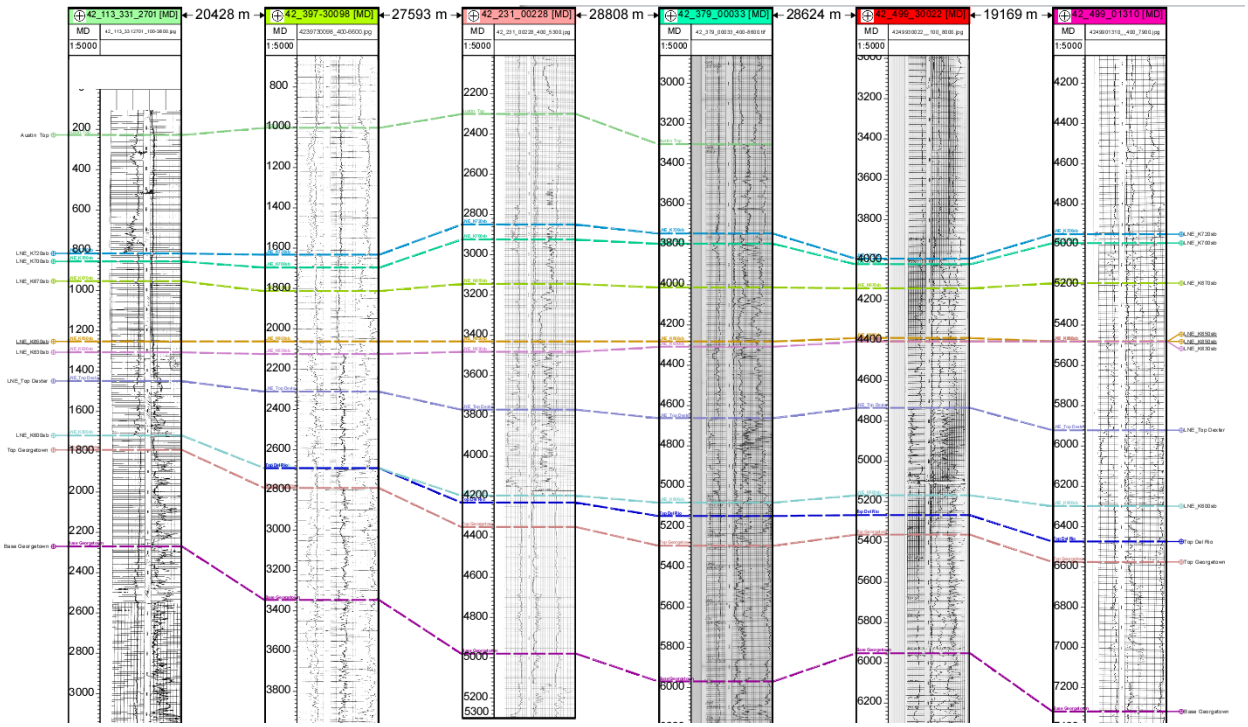

Above: EW700

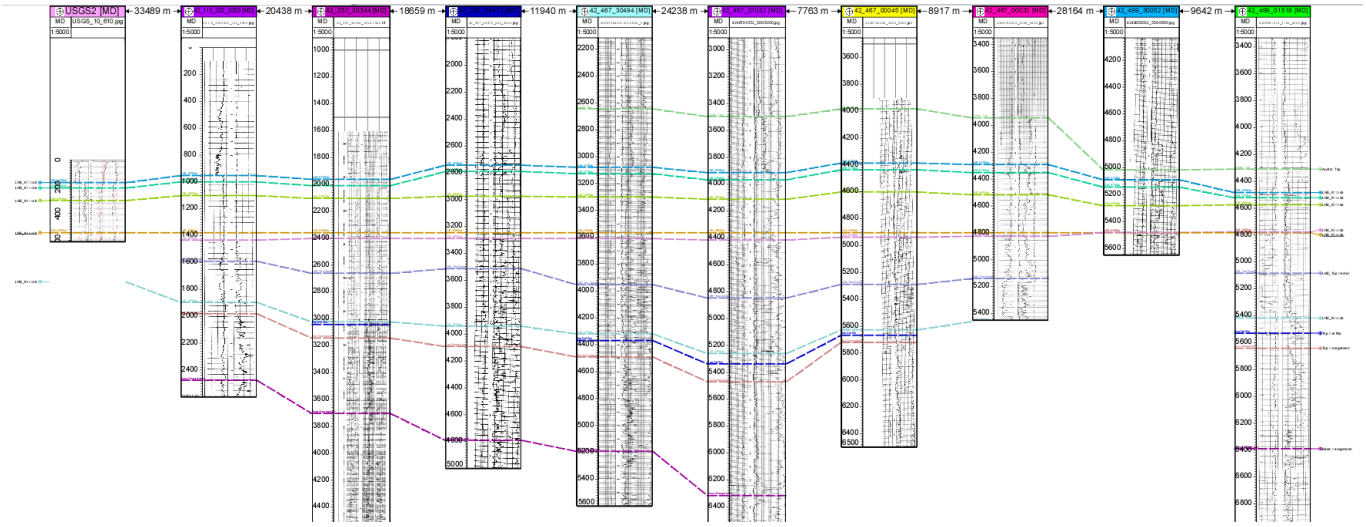

Above: EW800

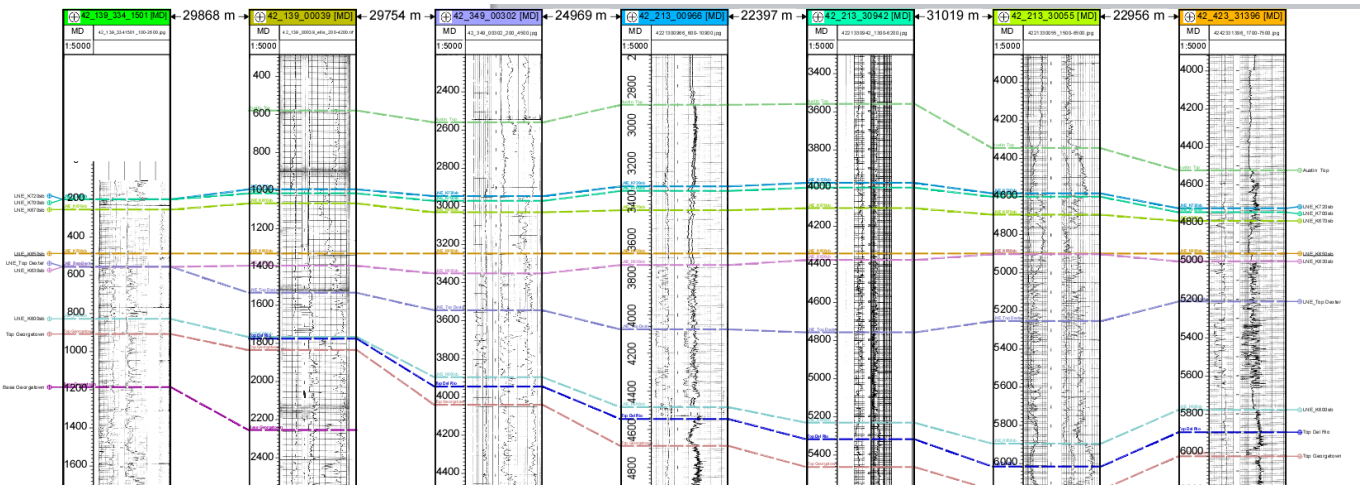

Above: EW1000

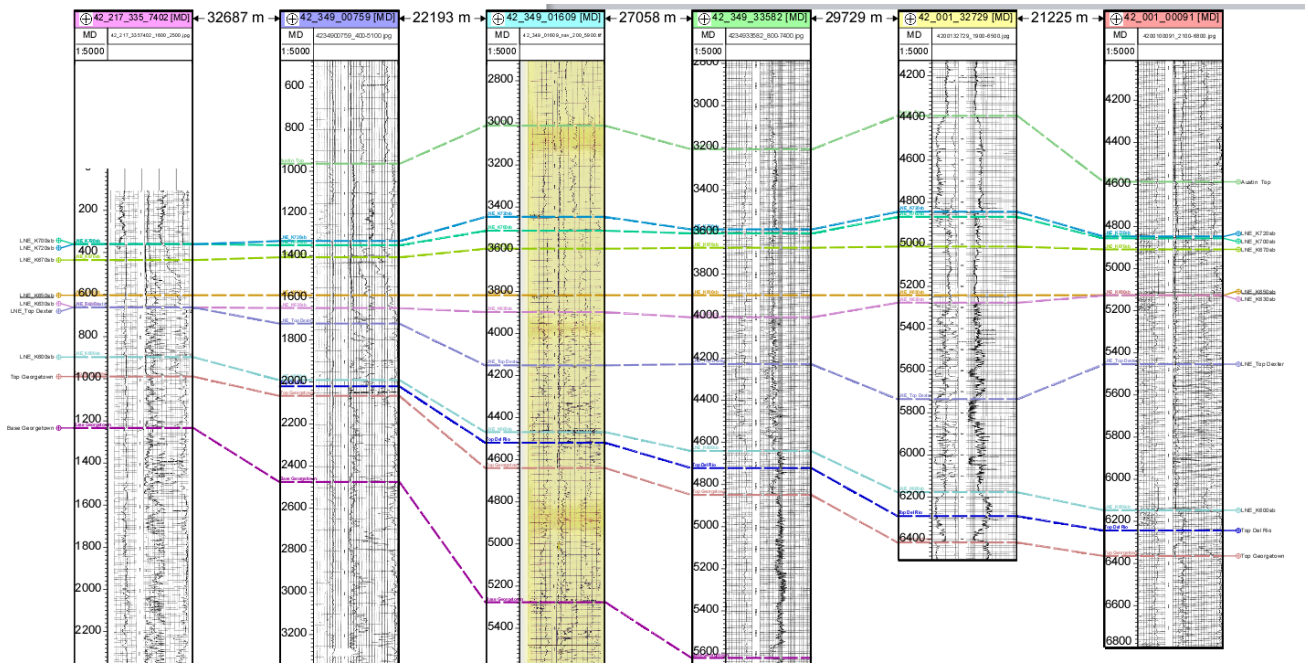

Above: EW1200

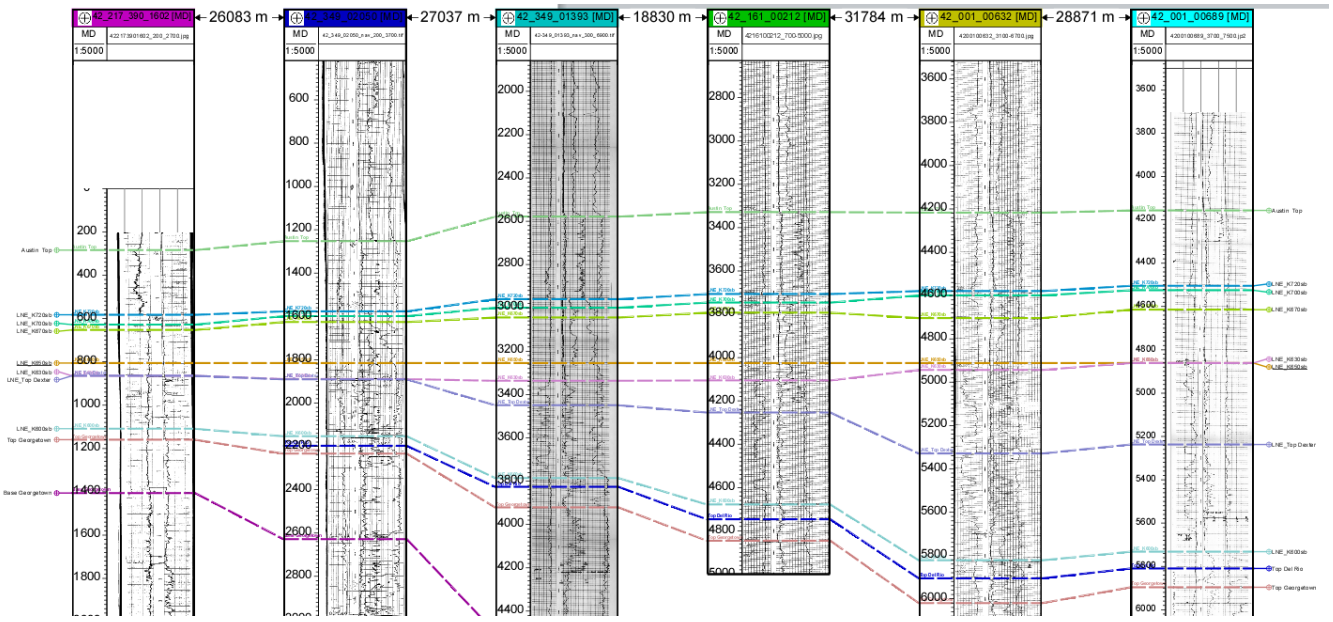

Above: EW1200

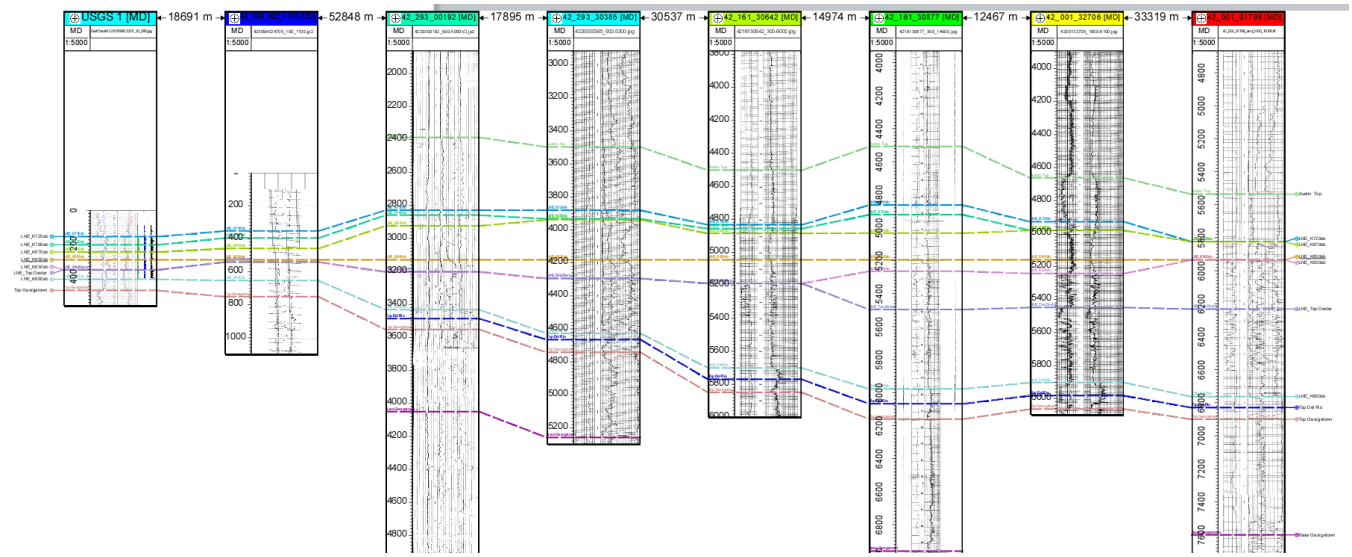

Above: EW1300

Name	Latitude (WGS 84)	Longitude (WGS 84)	LNE_K720sb	LNE_K700sb	LNE_K670sb	LNE_K650sb	LNE_K630sb	LNE_Top Dexter	LNE_K600sb	Top Del Rio	Top Georgetown
42_001_00091	32.055369	-95.564587	-4441.83	-4450.85	-4529.26	-4721.64	-4721.64	-5048.53	-5742.03	-5838.43	-5959.14
42_001_00632	31.85695	-95.81323	-4176.06	-4196.27	-4300.69	-4508.6	-4540.2	-4926.08	-5419.18	-5502.37	-5616.54
42_001_00689	31.894348	-95.511523	-4184.17	-4204.8	-4294.31	-4540.44	-4540.44	-4916.87	-5411.77	-5489.42	-5576.29
42_001_01798	31.591035	-95.446987	-5388.04	-5388.04	-5388.04	-5498.01	-5498.01	-5796.38	-6327.01	-6393.56	-6464.48
42_001_31855	31.86807	-95.50971	-4459.74	-4459.74	-4459.74	-4600.72	-4600.72	-4812.2	-5488.94	-5574.14	-5681
42_001_32706	31.632656	-95.794429	-4700.47	-4721.33	-4769.7	-4931.48	-4966.78	-5220.25	-5675.25	-5754.1	-5835.66
42_001_32729	32.034093	-95.787734	-4431.86	-4456.23	-4562.27	-4828.51	-4863.96	-5321.76	-5763.74	-5877.31	-6002.47
42_085_00038	33.096728	-96.544447	-249.44	-306.69	-436.73	-766.41	-766.41	-971.92	-1239.13	-1239.13	-1300.62
42_085_00055	33.04257	-96.44419	-602.87	-674.32	-784.47	-1117.9	-1117.9	-1317.36	-1650.78	-1650.78	-1752
42_113_330_4801	32.902222	-96.565277	-354.92	-390.98	-523.21	-825.21	-855.92	-1052.65	-1308.25	-1308.25	-1377.11
42_113_331_2701	32.77861	-96.602222	-293.76	-333.16	-437.29	-730.51	-754.91	-926.94	-1197.23	-1197.23	-1268.88
42_113_332_0303	32.71888	-96.536388	-629.87	-677.19	-770.75	-1055.8	-1110.41	-1268.37	-1573.69	-1573.69	-1658.9
42_139_00019	32.464	-96.62	-432.08	-461.59	-523.22	-807.62	-870.26	-950.15	-1287.15	-1287.15	-1344.44
42_139_00039	32.257947	-96.628637	-563.32	-584.37	-637.04	-900.01	-953.37	-991.18	-1346.59	-1346.59	-1405.95
42_139_14691	32.538333	-96.955555	623.63	595.84	493.94	292.9	244.67	244.67	-89.23	-89.23	-152.25
42_139_334_1501	32.3263889	-96.9352778	492.33	492.33	447.69	208.38	139.84	139.84	-154.8	-154.8	-213.64
42_161_00212	31.87355	-96.148339	-3354.35	-3393.75	-3440.49	-3673.24	-3719.44	-3901.49	-4326.03	-4394.77	-4493.4
42_161_30642	31.568353	-96.061993	-4400.9	-4424.01	-4453.37	-4613.84	-4654.61	-4757.41	-5269.1	-5337.84	-5417.16
42_161_30877	31.636235	-95.925692	-4512.56	-4570.99	-4603.92	-4758.51	-4808.94	-5145.87	-5626.87	-5717.26	-5810.21
42_213_00966	32.276408	-96.079268	-2920.54	-2944.6	-3014.12	-3272.84	-3328.45	-3670.06	-4077.86	-4140.24	-4281.54
42_213_30055	32.26474	-95.51309	-4182.18	-4199.76	-4299.21	-4497.67	-4497.67	-4851.72	-5494.62	-5614.65	-5737.97
42_213_30942	32.26546	-95.842038	-3477.4	-3502.77	-3607.14	-3848.17	-3881.41	-4261.48	-4735.05	-4821.74	-4967.34
42_217_335_7402	32.0425	-96.9638889	262.15	262.15	180.98	18.93	-38.64	-38.64	-274.86	-274.86	-367.11
42_217_390_1602	31.9175	-96.8959333	-85.53	-102.12	-186.77	-313.45	-357.52	-357.52	-616.58	-616.58	-667.22
42_223_00327	33.153694	-95.754809	-2857.27	-2906.58	-3220.93	-3459.78	-3484.43	-3826.52	-4199.42	-4253.56	-4364.3
42_231_00129	33.074677	-96.105831	-1500.38	-1529.66	-1684.88	-1958.23	-2023.45	-2318.49	-2720.67	-2720.67	-2796.76
42_231_00228	32.858889	-96.104445	-2411.65	-2486.05	-2653.16	-2992.27	-3017.34	-3330.78	-3757.14	-3791.97	-3913.09
42_231_00243	32.95646	-96.126982	-2134.49	-2185.39	-2369.83	-2677.63	-2749.06	-3036.33	-3419.21	-3460.25	-3593.79
42_257_00198	32.46006	-96.422972	-974.07	-1023.17	-1116.9	-1342.43	-1440.03	-1569.42	-1935.98	-1961.87	-2057.07

Name	Latitude (WGS 84)	Longitude (WGS 84)	LNE_K720sb	LNE_K700sb	LNE_K670sb	LNE_K650sb	LNE_K630sb	LNE_Top Dexter	LNE_K600sb	Top Del Rio	Top Georgetown
42_257_00472	32.724729	-96.176303	-2211.06	-2258.05	-2442.6	-2713.77	-2757.05	-2981.33	-3408.97	-3448.86	-3560.17
42_257_30266	32.50769	-96.09691	-2845.91	-2888.07	-2991.85	-3264.66	-3333.61	-3660.9	-4047.99	-4107.01	-4238.34
42_257_30344	32.633493	-96.34336	-1530.67	-1578.13	-1645.86	-1928.55	-1971.31	-2230.09	-2591.19	-2611.52	-2712.35
42_293_00192	31.658117	-96.548641	-2349.48	-2416.86	-2472.26	-2636.81	-2687.57	-2687.57	-2953.08	-3006.73	-3072.82
42_293_30385	31.580699	-96.383217	-3346.87	-3399.79	-3442.46	-3648.12	-3698.53	-3698.53	-4093.88	-4131.92	-4208.77
42_309_391_7701	31.658611	-96.9719444	-247.97	-277.33	-353.66	-586.03	-615.05	-806.8	-1044.92	-1044.92	-1132.9
42_309_402_4705	31.629721	-97.104722	132.31	84.2	40.06	-46.07	-103.47	-103.47	-167.95	-167.95	-266.02
42_349_00302	32.189506	-96.323523	-2520.19	-2545.28	-2604.76	-2821.32	-2870.33	-3118.69	-3469.82	-3518.76	-3614.29
42_349_00759	32.007783	-96.620333	-886.05	-919.89	-963.18	-1143.66	-1204.5	-1278.33	-1546.3	-1576.21	-1621.49
42_349_01393	31.880261	-96.347106	-2548.28	-2588	-2633.23	-2843.7	-2892.68	-3038.31	-3374.49	-3415.26	-3510.22
42_349_01609	32.035155	-96.387688	-3009.23	-3064.99	-3160.59	-3381.55	-3461.27	-3714.48	-4031.68	-4081.98	-4202.54
42_349_02050	31.852825	-96.630915	-1077.36	-1124.8	-1178.37	-1316.25	-1348.21	-1348.21	-1654.16	-1698.39	-1788.38
42_349_33582	32.04906	-96.1018	-3262.01	-3280.62	-3349.27	-3574.8	-3679.72	-3901.96	-4314.33	-4395.8	-4523.03
42_379_00033	32.809084	-95.802652	-3291.54	-3342.18	-3559.45	-3814.21	-3814.21	-4207.73	-4627.2	-4693.57	-4840.94
42_397-30098	32.84452	-96.3986	-1083.91	-1147.88	-1264.39	-1522.55	-1550.62	-1763.55	-2143.71	-2143.71	-2242.05
42_423_00477	32.496189	-95.285839	-4190.67	-4207.89	-4289.2	-4496.45	-4496.45	-4830.54	-5394.3	-5471.17	-5603.11
42_423_30428	32.484469	-95.536628	-4274.31	-4300.04	-4427.12	-4610.4	-4610.4	-4982.11	-5563.47	-5648.68	-5783.26
42_423_31396	32.27653	-95.27008	-4181.68	-4202.6	-4248.07	-4418.4	-4418.4	-4670.51	-5238.61	-5355.96	-5481.96
42_467_00032	32.654632	-95.624508	-3883.84	-3943.64	-4108.57	-4391.27	-4417.12	-4731.4	-5051.09	-5051.09	x
42_467_00045	32.652579	-95.71945	-3924.39	-3974.3	-4139.23	-4442.85	-4476.09	-4827.16	-5165.33	-5205.95	-5258.87
42_467_01032	32.675366	-95.797632	-3435.74	-3489.39	-3633.75	-3883.1	-3937.18	-4368.4	-4781.63	-4858.86	-4991.83
42_467_30494	32.69161	-96.055199	-2590.99	-2638.19	-2776.07	-3077.98	-3121.51	-3463.83	-3830.49	-3880.14	-4002.22
42_467_30833	32.380318	-95.874849	-3488.84	-3514.62	-3642.01	-3943.98	-3990.25	-4355.74	-4855.29	-4952.51	-5096.01
42_467_30844	32.48071	-95.85105	-3711.83	-3742.34	-3879.49	-4180.21	-4202.52	-4606.31	-5102.17	-5170.97	-5308.15
42_467_31041	32.403659	-95.524702	-4222.78	-4243.22	-4328.83	-4590.29	-4590.29	-4902.26	-5501.06	-5629.53	-5760.19
42_499_01518	32.58736	-95.232165	-4153.17	-4191.43	-4261.45	-4446.44	-4446.44	-4753.15	-5087	-5199.75	-5312.08
42_499_30022	32.833595	-95.498602	-3546.88	-3574.28	-3740.88	-3910.18	-3910.18	-4287.46	-4721.54	-4819.76	-4917.06
42_499_30052	32.619337	-95.327558	-4759.42	-4813.77	-4951.79	-5151.73	-5151.73	x	x	x	x
USGS 1	31.495	-97.22306	519.21	469.4	441.05	379.82	317.15	317.15	260.51	260.51	193.34
USGS2	32.6913	-96.892	540.02	499.95	406.34	166.92	x	x	x	x	x

Above: SSTVD Values for sequence stratigraphic surfaces (feet)

Name	Latitude (WGS 84)	Longitude (WGS 84)	UM_UEF	MM_UEF	LM_UEF	LEF	EF	WB	Lewisville	Dexter	Buda	Del Rio
USGS 1	31.495	-97.22306	49.8	28.4	61.2	62.7	202.1	56.6	0	56.6	x	x
42_309_402_4705	31.629721	-97.104722	48.1	44.1	86.1	57.4	235.8	64.5	0	64.5	0	98.1
42_309_391_7701	31.658611	-96.9719444	29.4	76.3	232.4	29	367.1	429.9	191.8	238.1	0	88
42_217_335_7402	32.0425	-96.9638889	0	81.2	162.1	57.6	300.8	236.2	0	236.2	0	92.3
42_139_14691	32.538333	-96.955555	27.8	101.9	201	48.2	379	333.9	0	333.9	0	63
42_139_334_1501	32.3263889	-96.9352778	0	44.6	239.3	68.5	352.5	294.6	0	294.6	0	58.8
42_217_390_1602	31.9175	-96.8959333	16.6	84.7	126.7	44.1	272	259.1	0	259.1	0	50.6
USGS2	32.6913	-96.892	40.1	93.6	239.4	x	x	x	x	x	x	x
42_349_02050	31.852825	-96.630915	47.4	53.6	137.9	32	270.9	306	0	306	44.2	90
42_139_00039	32.257947	-96.628637	21.1	52.7	263	53.4	390.1	393.2	37.8	355.4	0	59.4
42_349_00759	32.007783	-96.620333	33.8	43.3	180.5	60.8	318.5	341.8	73.8	268	29.9	45.3
42_139_00019	32.464	-96.62	29.5	61.6	284.4	62.6	438.2	416.9	79.9	337	0	57.3
42_113_331_2701	32.77861	-96.602222	39.4	104.1	293.2	24.4	461.2	442.3	172	270.3	0	71.7
42_113_330_4801	32.902222	-96.565277	36.1	132.2	302	30.7	501	452.3	196.7	255.6	0	68.9
42_293_00192	31.658117	-96.548641	67.4	55.4	164.6	50.8	338.1	265.5	0	265.5	53.7	66.1
42_085_00038	33.096728	-96.544447	57.3	130	329.7	0	517	472.7	205.5	267.2	0	61.5
42_113_332_0303	32.71888	-96.536388	47.3	93.6	285.1	54.6	480.5	463.3	158	305.3	0	85.2
42_085_00055	33.04257	-96.44419	71.5	110.2	333.4	0	515	532.9	199.5	333.4	0	101.2
42_257_00198	32.46006	-96.422972	49.1	93.7	225.5	97.6	466	496	129.4	366.6	25.9	95.2
42_397-30098	32.84452	-96.3986	64	116.5	258.2	28.1	466.7	593.1	212.9	380.2	0	98.3
42_349_01609	32.035155	-96.387688	55.8	95.6	221	79.7	452	570.4	253.2	317.2	50.3	120.6
42_293_30385	31.580699	-96.383217	52.9	42.7	205.7	50.4	351.7	395.4	0	395.4	38	76.9
42_349_01393	31.880261	-96.347106	39.7	45.2	210.5	49	344.4	481.8	145.6	336.2	40.8	95
42_257_30344	32.633493	-96.34336	47.5	67.7	282.7	42.8	440.6	619.9	258.8	361.1	20.3	100.8
42_349_00302	32.189506	-96.323523	25.1	59.5	216.6	49	350.1	599.5	248.4	351.1	48.9	95.5
42_257_00472	32.724729	-96.176303	47	184.6	271.2	43.3	546	651.9	224.3	427.6	39.9	111.3
42_161_00212	31.87355	-96.148339	39.4	46.7	232.8	46.2	365.1	606.6	182.1	424.5	68.7	98.6
42_231_00243	32.95646	-96.126982	50.9	184.4	307.8	71.4	614.6	670.2	287.3	382.9	41	133.5
42_231_00129	33.074677	-96.105831	29.3	155.2	273.4	65.2	523.1	697.2	295	402.2	0	76.1

Name	Latitude (WGS 84)	Longitude (WGS 84)	UM_UEF	MM_UEF	LM_UEF	LEF	EF	WB	Lewisville	Dexter	Buda	Del Rio
42_231_00228	32.858889	-96.104445	74.4	167.1	339.1	25.1	605.7	739.8	313.4	426.4	34.8	121.1
42_349_33582	32.04906	-96.1018	18.6	68.7	225.5	104.9	417.7	634.6	222.2	412.4	81.5	127.2
42_257_30266	32.50769	-96.09691	42.2	103.8	272.8	69	487.7	714.4	327.3	387.1	59	131.3
42_213_00966	32.276408	-96.079268	24.1	69.5	258.7	55.6	407.9	749.4	341.6	407.8	62.4	141.3
42_161_30642	31.568353	-96.061993	23.1	29.4	160.5	40.8	253.7	614.5	102.8	511.7	68.7	79.3
42_467_30494	32.69161	-96.055199	47.2	137.9	301.9	43.5	530.5	709	342.3	366.7	49.7	122.1
42_161_30877	31.636235	-95.925692	58.4	32.9	154.6	50.4	296.4	817.9	336.9	481	90.4	92.9
42_467_30833	32.380318	-95.874849	25.8	127.4	302	46.3	501.4	865	365.5	499.6	97.2	143.5
42_467_30844	32.48071	-95.85105	30.5	137.2	300.7	22.3	490.7	899.7	403.8	495.9	68.8	137.2
42_213_30942	32.26546	-95.842038	25.4	104.4	241	33.2	404	853.6	380.1	473.6	86.7	145.6
42_001_00632	31.85695	-95.81323	20.2	104.4	207.9	31.6	364.1	879	385.9	493.1	83.2	114.2
42_379_00033	32.809084	-95.802652	50.6	217.3	254.8	0	522.7	813	393.5	419.5	66.4	147.4
42_467_01032	32.675366	-95.797632	53.7	144.4	249.4	54.1	501.4	844.5	431.2	413.2	77.2	133
42_001_32706	31.632656	-95.794429	20.9	48.4	161.8	35.3	266.3	708.5	253.5	455	78.9	81.6
42_001_32729	32.034093	-95.787734	24.4	106	266.2	35.4	432.1	899.8	457.8	442	113.6	125.2
42_223_00327	33.153694	-95.754809	49.3	314.4	238.9	24.6	627.2	715	342.1	372.9	54.1	110.7
42_467_00045	32.652579	-95.71945	49.9	164.9	303.6	33.2	551.7	689.2	351.1	338.2	40.6	52.9
42_467_00032	32.654632	-95.624508	59.8	164.9	282.7	25.8	533.3	634	314.3	319.7	x	x
42_001_00091	32.055369	-95.564587	9	78.4	192.4	0	279.8	1020.4	326.9	693.5	96.4	120.7
42_423_30428	32.484469	-95.536628	25.7	127.1	183.3	0	336.1	953.1	371.7	581.4	85.2	134.6
42_467_31041	32.403659	-95.524702	20.4	85.6	261.5	0	367.5	910.8	312	598.8	128.5	130.7
42_213_30055	32.26474	-95.51309	17.6	99.4	198.5	0	315.5	997	354.1	642.9	120	123.3
42_001_00689	31.894348	-95.511523	20.6	89.5	246.1	0	356.3	871.3	376.4	494.9	77.6	86.9
42_001_31855	31.86807	-95.50971	0	0	141	0	141	888.2	211.5	676.7	85.2	106.9
42_499_30022	32.833595	-95.498602	27.4	166.6	169.3	0	363.3	811.4	377.3	434.1	98.2	97.3
42_001_01798	31.591035	-95.446987	0	0	110	0	110	829	298.4	530.6	66.6	70.9
42_499_30052	32.619337	-95.327558	54.4	138	199.9	0	392.3	x	x	x	x	x
42_423_00477	32.496189	-95.285839	17.2	81.3	207.3	0	305.8	897.9	334.1	563.8	76.9	131.9
42_423_31396	32.27653	-95.27008	20.9	45.5	170.3	0	236.7	820.2	252.1	568.1	117.4	126
42_499_01518	32.58736	-95.232165	38.3	70	185	0	293.3	640.6	306.7	333.9	112.8	112.3

Above: Isochore thicknesses for stratigraphic units (feet)